JOURNAL OF GEOPHYSICAL RESEARCH, VOL. 94, NO. C12, PAGES 18,095–18,117, DECEMBER 15, 1989

Interannual Variability in Phytoplankton Pigment Distribution During the Spring Transition Along the West Coast of North America

A. C. THOMAS AND P. T. STRUB

College of Oceanography, Oregon State University, Corvallis

A 5-year time series of coastal zone color scanner imagery (1980–1983, 1986) is used to examine changes in the large-scale pattern of chlorophyll pigment concentration coincident with the spring transition in winds and currents along the west coast of North America. The data show strong interannual variability in the timing and spatial patterns of pigment concentration at the time of the transition event. In both 1980 and 1981 a large increase in pigment concentration occurs (from 0.5 mg m^{-3} to >3.0 mg m^{-3} in 1980 and from 0.3 mg m^{-3} to >1.5 mg m^{-3} in 1981). In these years, as well as in 1982, the increase takes place between ≈33°N and ≈41°N, but it occurs in a region centered 300 km offshore in 1980 and within 300 km of the coast in 1981 and 1982. These changes are in contrast to 1983 and 1986, when virtually no change in pattern or concentration is associated with the transition. Calculations of light availability and in situ data suggest this region is nutrient limited even in the mid to late winter. Time series of pigment concentration and wind forcing for extended periods before and after the transition date show that increases in concentration are associated with strong wind mixing events prior to the transition and with the onset of southward wind stress (upwelling) at the time of the transition. Interannual variability in the response of pigment concentration to the spring transition appears to be a function of spatial and temporal variability in vertical nutrient flux induced by wind mixing and/or the upwelling initiated at the time of the transition. Interannual differences in the mixing regime are illustrated with a one-dimensional mixing model.

1. INTRODUCTION

A spring transition in wind and current structure off the west coast of North America marks the end of the winter regime of northward mean flow within the California Current System (CCS) and the beginning of the summer regime characterized by upwelling and southward flow [*Hickey*, 1979]. This transition usually occurs quite rapidly, often over the course of a few days [*Huyer et al.*, 1979; *Breaker and Mooers*, 1986], with large alongshore length scales of 500 to 2000 km [*Strub et al.*, 1987*a*].

Biological responses to this physical transition and the sudden switch to a mean upwelling-favorable wind have not been investigated. The short time and large spatial scales over which the transition occurs preclude the possibility of adequately mapping chlorophyll distributions during the event with data from ship cruises. The availability of satellite estimates of surface pigment concentration from the coastal zone color scanner (CZCS) on Nimbus 7, however, allows a synoptic representation of these patterns at the time of the transition with the necessary space and time scales.

We analyze CZCS data from 5 years (1980–1983 and 1986) to determine if large-scale changes in near-surface pigment distribution take place in association with the spring transition event. We present the major differences and similarities between years and relate our observations to large-scale forcing mechanisms in an attempt to explain the observed patterns of concentration and interannual variability. In section 2 we provide a brief description of the physical spring transition event and a synopsis of the biological and physical regimes within the CCS during winter and summer. A description of the satellite data and their treatment and of other data sets used in the study is given in section 3. In section 4, spatial patterns of pigment concentration from the spring transition period are presented together with temporal patterns of concentration over periods extending before and after the transition. These patterns are discussed in relation to large-scale forcing in section 5, using wind data, calculations of incident solar radiation, and available in situ profiles of density, chlorophyll, and nutrient concentrations. Section 6 contains a summary and conclusions of these results.

Paper number 89JC01398.
0148-0227/89/89JC-01398$05.00

2. BACKGROUND

The physical spring transition is a response to large-scale wind forcing [*Huyer et al.*, 1979; *Strub et al.*, 1987*a*; *Strub and James*, 1988]. As the winter Aleutian low-pressure system weakens and moves northwestward, the North Pacific high-pressure system and a low-pressure system over the southwestern United States strengthen, changing the dominant winds from northward to southward over the continental margin. This southward wind stress results in an offshore Ekman transport and the onset of the well-documented summer upwelling regime along the west coast, with lower coastal sea levels, southward surface currents and a strong cross-shelf density gradient [*Huyer*, 1983]. The strength of this oceanic response is greatest north of approximately 35°–37°N [*Strub et al.*, 1987*a*]. South of this latitude, the event is weak or not present; here the monthly mean wind stress is southward all year and the seasonal change in sea level is small [*Strub et al.*, 1987*b*]. The physical spring transition typically takes place between mid-March and the end of April and can usually be identified as a rapid drop in coastal sea level over a few days, with levels remaining low thereafter.

Winter chlorophyll distributions within the full extent of the CCS are not well documented. Available data provide a broad-scale picture of pretransition conditions. Early winter (November–December) surface concentrations in the northward flowing Davidson Current off the southern British Columbia coast are <0.2 mg m^{-3} [*Thomas and Emery*, 1986,

1988]. *Landry et al.* [1989] show that the long-term mean (1954–1984) surface chlorophyll concentration off the Washington and Oregon coasts in late winter is ≈1.0 mg m^{-3}. Midwinter (January) surface concentrations from the southern portion of the study area (≈34°N) decrease from ≈1.0 mg m^{-3} nearshore to less than 0.2 mg m^{-3} in regions greater than 300 km offshore [*Haury et al.*, 1986]. This gradient is also observed in satellite images of the same area [*Smith et al.*, 1988]. In winter, the vertical distribution of chlorophyll is often uniform with depth, and the thermocline is relatively deep (≈75 m) [*Michaelsen et al.*, 1988] in the central and southern California region. These authors show that in spring, the water column stratifies and a subsurface chlorophyll maximum develops. *Eppley et al.* [1985] point out that ship data show that total water column production in the Southern California Bight does not show a seasonal cycle but that chlorophyll concentration in the upper attenuation depth of the euphotic zone (that region sampled by the CZCS) has a winter maximum and summer minimum. A portion of this seasonality observed in CZCS data is a result of much of the summer production and biomass occurring as a subsurface chlorophyll maximum, below the depth sampled by the satellite sensor (as discussed by *Campbell and O'Reilly* [1988]), and shown by *Michaelsen et al.* [1988]. These authors show that the amplitude of this annual cycle is largest in offshore regions and relatively small within 100 km of the coast in the central California region. A winter maximum is not evident in ship data off the Oregon and Washington coasts [*Landry et al.*, 1989].

Summer distributions of chlorophyll in the CCS have been more fully documented and illustrate the characteristics of the region after the transition. Using comparisons of critical depth and the depth of mixing, *Parsons et al.* [1966] show the onset of the spring bloom in the North Pacific can start at latitudes less than ≈45°N in February and move northwestward. Summer coastal distributions are characterized by strong temporal and spatial variability closely related to wind stress and resultant upwelling [*Small and Menzies*, 1981; *Abbott and Zion*, 1985] and along-shelf and cross-shelf advection [*Abbott and Zion*, 1987]. These studies show a general trend of high biomass near the coast in the upwelling zones, decreasing offshore to the oligotrophic conditions of central Pacific water. Mean summer surface concentrations of greater than 2.5 mg m^{-3} are found in coastal regions off central California, with concentrations less than 0.5 mg m^{-3} in regions farther than ≈250 km from shore [*Smith et al.*, 1988]. These authors state that spatial patterns offshore are dominated by larger-scale variability than those nearshore, and biomass is consistently lower. Variability in both concentration and spatial patterns is maximum in the early summer [*Barale and Fay*, 1986]. *Chelton et al.* [1982] and *Chelton* [1982] argue that the large-scale biological variability in offshore regions within the CCS is coupled more closely to changes in southward advection and wind stress curl than to coastal upwelling.

3. Data Preparation

The CZCS images utilized in this study are part of the West Coast Time Series. They were recorded at the Scripps Satellite Oceanography Facility (La Jolla, California) and processed at the Jet Propulsion Laboratory (Pasadena, California) with software developed by O. Brown and R. Evans (University of Miami). Atmospheric correction was done with coefficients found by *Gordon et al.* [1983*a*, *b*]. The images were initially navigated into square 512 × 512 pixel images with spatial resolutions of 100 pixels per degree. Each of these original images from a single satellite pass over the west coast of North America was then subsampled and combined to form a 512 × 512 pixel image of the entire west coast (≈22°N to 55°N) with a spatial resolution of ≈14.3 pixels per degree. Radiance measured by the CZCS was processed to yield values of pigment concentration. The accuracy of the CZCS pigment measurements is estimated to be log [Chlorophyll] ± 0.5 [*Gordon et al.*, 1980]. Tests by *Smith et al.* [1988] showed the accuracy of the CZCS data when compared with ship data from the southern California coast was ≈ ±40% for pigment values ranging from 0.05 to 10.0 mg m^{-3}. *Abbott and Zion* [1987] reported a regression of log-transformed satellite pigment on ship chlorophyll to have an r^2 of 0.8 and a slope of 1.0 in the coastal region of the CCS off northern California.

TABLE 1. The Spring Transition Date

Year	Date
1980	March 22
1981	March 26
1982	April 18
1983	April 4
1986	March 17

The transition date in each year is defined here as the spring date when sea levels at 41.8°N (Crescent City tide gauge data) drop rapidly in a period of a few days and stay low. The alongshore coherence of this date for each year was confirmed with sea level data from tidal stations north and south of this station. *Strub et al.* [1987*a*] show that this location and procedure are a reasonable signature of the event over the study area and that the date of the transition varied between March 22 and April 18 for the 9 years of data which they examined. The date of the spring transition in each of the years studied here is given in Table 1.

Visual inspection of the available images from the spring transition period in each year indicates that cloud cover is too widespread for single images to depict pigment distributions before or after the actual event. In addition, very few images were recorded during 1984 and 1985 owing to problems on the satellite, so descriptive and statistical analysis of the spring transition is restricted to the 5-year time series 1980–1983 and 1986. Cloud cover even in these years results in large spatial gaps in the data (see also *Kelly* [1985], *Abbott and Zion* [1987], and *Michaelsen et al.* [1988]). To fill these gaps, we have formed composite images over periods centered about the spring transition date. Following the procedure of *Strub et al.* [1987*a*], we identify the date of the physical transition in each year from time series of coastal sea level data and then form temporal composites over both 10- and 15-day periods before and after this date. Pigment concentrations for each pixel in these composites are calculated by averaging over all available images within the time period without including cloud-contaminated pixels. To reduce the effect of single images and outlying pixel values, a concentration is assigned to pixels only if there were at least two representations within the time period. Pixels failing this criterion are flagged as cloud. The 10- and 15-day periods

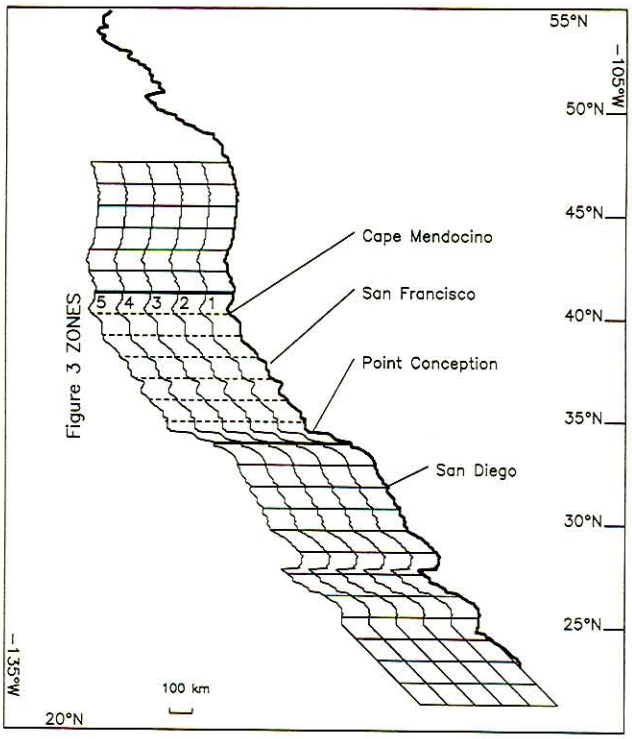

Fig. 1. A coastal outline of the study area showing major geographic points. The 100 × 100 km regions over which pigment from each 15-day composite was averaged to produce the spatial points for input into the EOF calculation are shown. Also shown are the northern and southern boundaries (bold lines) of the five 100-km-wide zones in the northern–central California region over which pigment concentrations in the 10-day composites were averaged to produce a time series in each year for Figure 3.

were chosen as a compromise between filling the spatial gaps by temporal averaging and retaining temporal resolution about the transition event. The 15-day composites are used to illustrate spatial patterns of pigment concentration, and a time series of 10-day composites is used to show temporal changes in concentration in selected regions.

The algorithm used to correct these images for atmospheric (Rayleigh) scattering is known to produce artificially high values of pigment concentration in regions of large solar zenith angle. Thus pigment concentrations estimated by the CZCS at high latitudes during winter cannot be trusted. Although reduction of this problem is now possible in the raw data processing [*Gordon et al.*, 1988], the West Coast Time Series were processed with a previous algorithm. For this reason, patterns of pigment off northern Oregon, Washington, and British Columbia for this spring period will not be interpreted or described. In this study we concentrate on patterns between approximately 23°N and 43°N.

Three other archived data sets are used for comparison with the satellite images. The central and southern portions of our study area (Figure 1) coincide with vertical profiles of temperature, salinity, chlorophyll, and nitrate obtained during California Cooperative Oceanic Fisheries Investigations, (CalCOFI) cruises [*Scripps Institution of Oceanography (SIO)*, 1985]. Daily wind velocities are available for grid points over the study area as part of the limited-area fine mesh (LFM) wind product of the National Meteorological Center, Washington, D. C. Daily observations of cloud cover collected by ships of opportunity are available in the Comprehensive Ocean Atmosphere Data Set (COADS) [*Woodruff et al.*, 1987]. These are used to estimate solar radiation.

4. Results

4.1. *Spatial Patterns Before and After the Transition*

CZCS image composites formed from the 15-day periods before and after the spring transition date in each year are shown in Plate 1. These 5 years show strong interannual variability in the response of pigment patterns to the transition event.

Two spatial patterns are common to all years. First, pigment concentrations are relatively high (>1.0 mg m^{-3}) within 50 km of the coast throughout the study area both before and after the transition event. In general, this shelf-slope region does not show any large-scale response to the transition event. *Barale and Fay* [1986] also show that high pigment values in regions nearest the coast are maintained throughout the year and show relatively little seasonal and interannual variability. High pigment values after the transition are an expected product of an upwelling regime [*Abbott and Zion*, 1985]. The higher pigment values prior to the transition adjacent to the coast are most likely supported by both episodic upwelling events which can occur even in winter [*Huyer*, 1983] and by interactions of bathymetry with tidal and other currents, all of which can lead to trophic enrichment of the shelf region [*Barale and Fay*, 1986]. Turbidity in the upper water column probably also contributes to the continually high satellite pigment estimates in this region closest to the coast. The effects of case 2 water are discussed further at the end of section 4.2. The second pattern common to each of the years is a negligible change in pigment patterns at the time of the transition in the southern portion of the study area. South of ≈33°N, the region of higher pigment concentrations (>1.0 mg m^{-3}) remains within ≈100 km of the coast both before and after the transition with no offshore expansion after the transition date. This is coincident with the region where the spring transition in physical processes is small or nonexistent [*Strub et al.*, 1987*a*].

The 15-day composites for 1980 (Figure 2*a*) show that large changes in pigment concentration occur at the time of the transition in the region between ≈43°N and ≈33°N. Pretransition pigment concentrations above 1.0 mg m^{-3} are generally restricted to within 150 km of the coast. After the transition, concentrations exceeding 3.0 mg m^{-3} occupy regions up to 500 km from the coast with the tongues extending 750 km offshore. The alongshore extent of this increase is difficult to estimate owing to cloud cover in the north, but a strong front perpendicular to the shore at approximately 33°N separates these high concentrations from concentrations of less than 0.5 mg m^{-3} to the south. Maximum change in pigment concentration at the time of the transition is within a broad region centered ≈300 km from shore with an alongshore length scale greater than 600 km. In this region of maximum change, pigment concentrations increase from ≈0.5 mg m^{-3} to greater than 3.0 mg m^{-3} in an average of 15 days over an area of ≈300,000 km^2.

Pigment patterns during the 1981 transition (Plate 1*b*) show an increase in concentration of similar alongshore

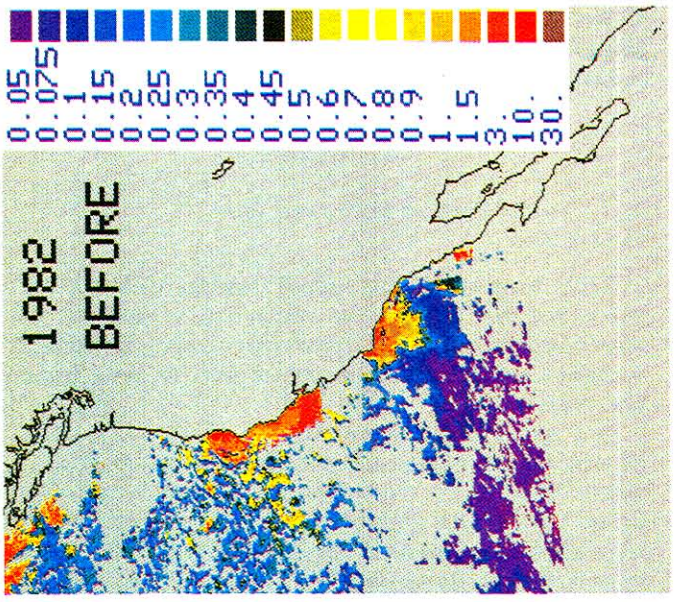

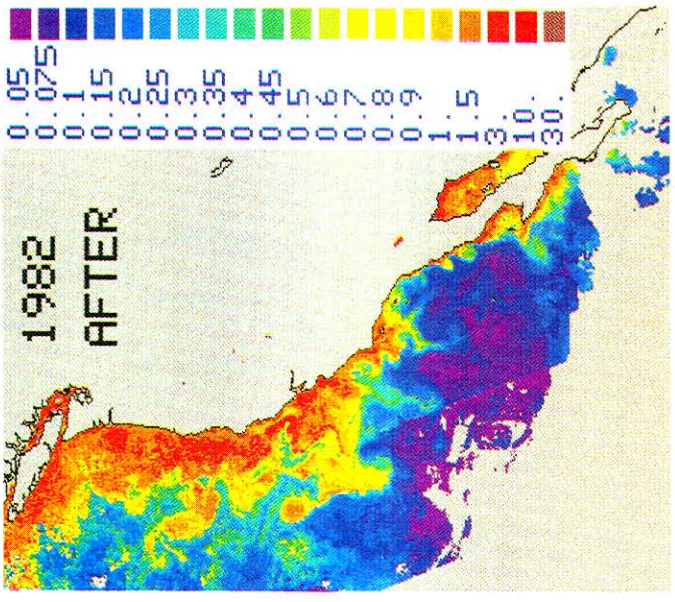

Plate 1c

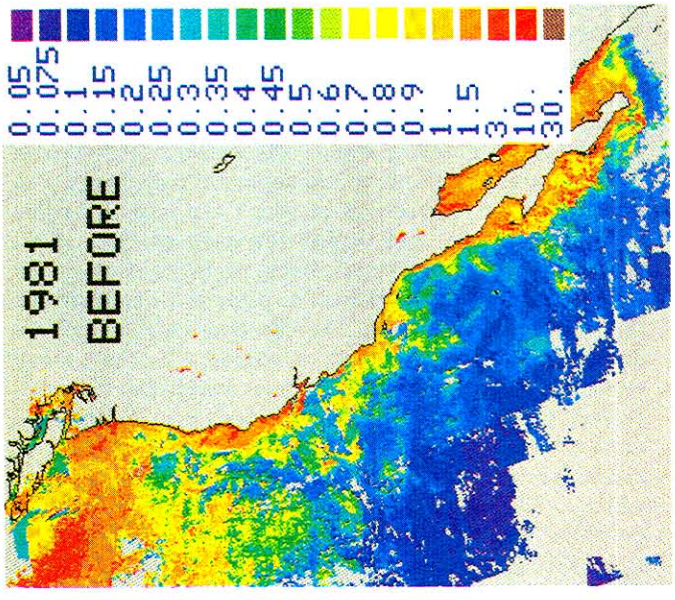

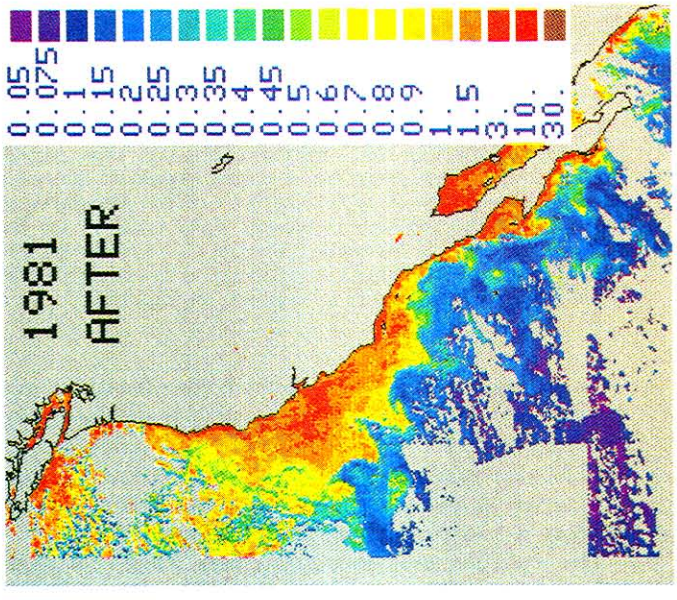

Plate 1b

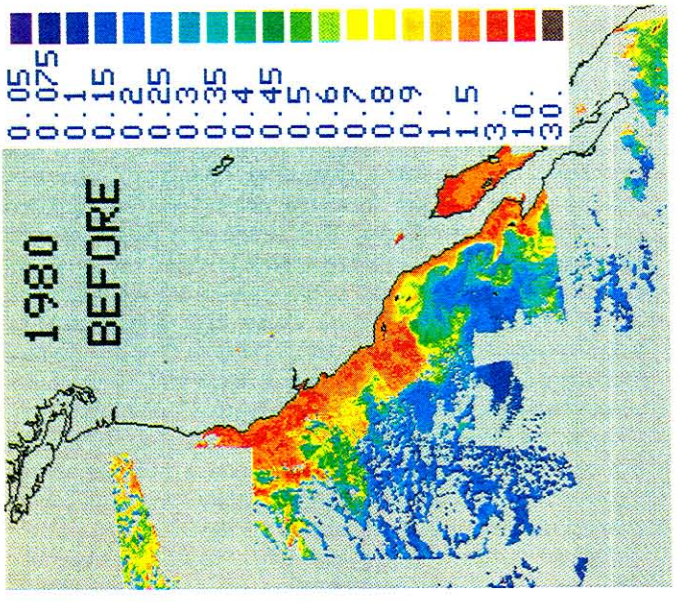

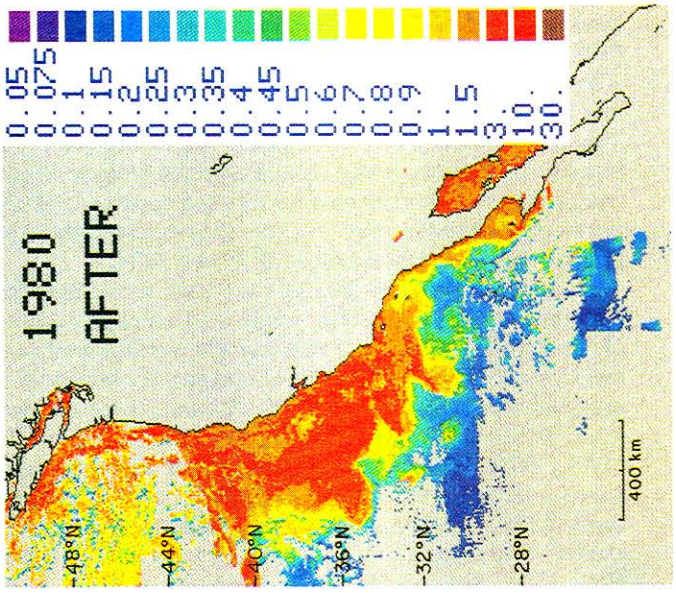

Plate 1a

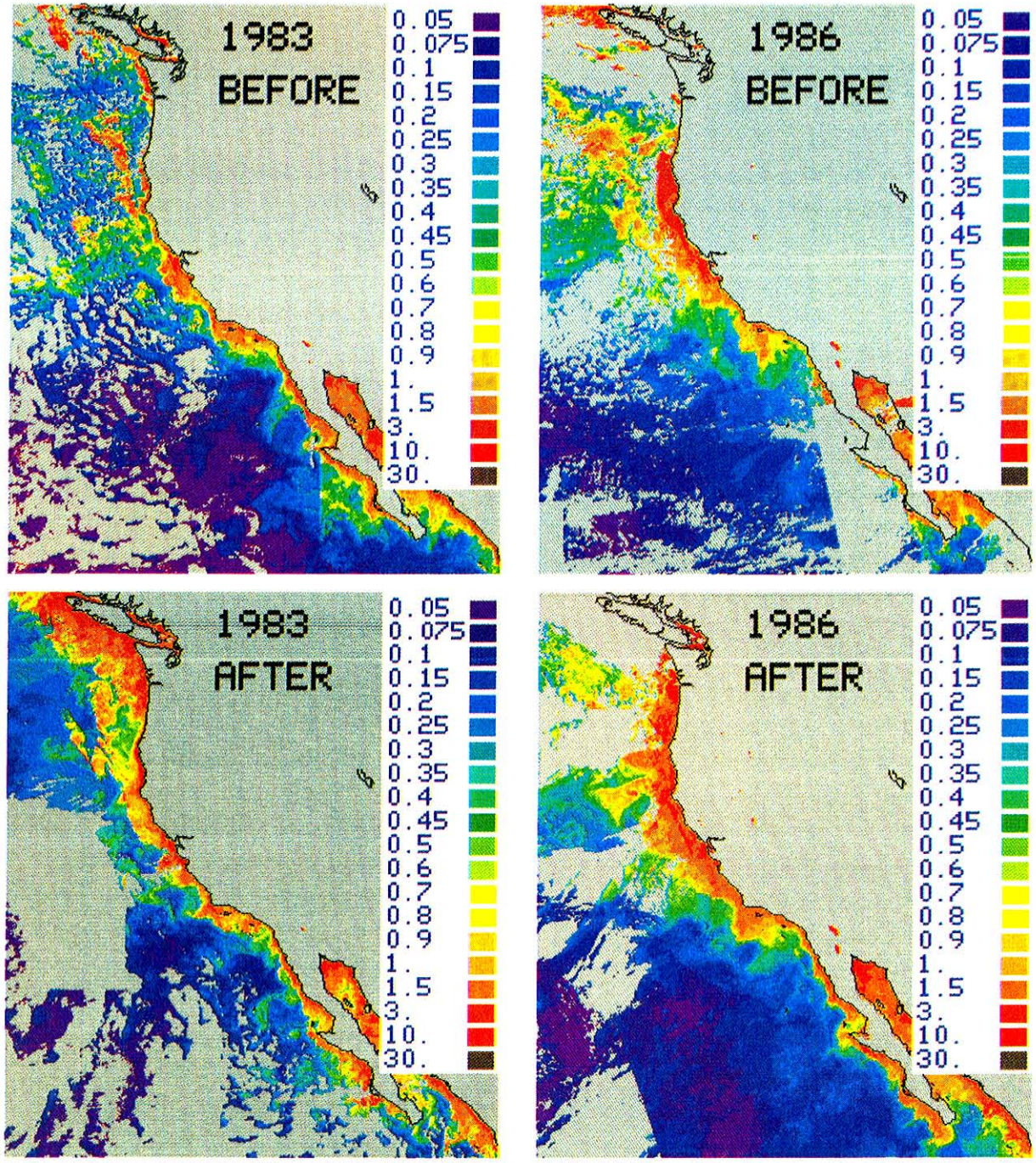

Plate 1. Image composites of coastal zone color scanner data of the California Current System in spring. Patterns of mean pigment concentration over 15-day periods (top) before and (bottom) after the physical spring transition dates (see Table 1) in each year are shown; years and the transition date in each are (*a*) 1980, March 22; (*b*) 1981, March 26; (*c*) 1982, April 18; (*d*) 1983, April 4; and (*e*) 1986, March 17. Regions north of ≈42°N are strongly influenced by the failure of the atmospheric correction algorithm and are not interpreted in this study.

length scales as the 1980 event. The maximum change in concentration, however, is more closely associated with the coast, in a region from ≈50 km to ≈300 km offshore. The large-scale change in concentration during the 1981 event is from ≈0.3 mg m^{-3} to ≈1.5 mg m^{-3} over a region of ≈180,000 km^2.

Changes in pigment patterns associated with the 1982 transition (Plate 1*c*) are of a different character than those previously seen. Prior to the transition (as well as can be visualized through the clouds), distributions in 1982 appear similar to 1980 and 1981. After the transition, however, the offshore increase in concentration shows considerably more spatial variability than was present in previous years and does not extend south of ≈35°N. Offshore concentrations greater than 1.0 mg m^{-3} are developed into eddy and jetlike features more closely resembling those previously described in association with summer upwelling periods for this region [*Abbott and Zion*, 1985, 1987; *Pelaez and McGowan*, 1986] than the broad-scale, diffuse increases seen after the 1980 and 1981 transitions.

There is virtually no change in pigment pattern associated with the physical spring transition in 1983 (Plate 1*d*). Concentrations of ≈1.0 mg m^{-3} within 100 km of the coast are present both before and after the transition. This concentration does not increase, and an offshore expansion of the region of higher concentrations occurs only in the relatively restricted region within 100 km of the shore between San Francisco Bay and Cape Mendocino. This lack of response to the spring transition is repeated in 1986 (Plate 1*e*). Pigment concentrations before and after the event are higher than those in 1983 within the coastal region (≈1.5 mg m^{-3}), and they extend farther from shore (≈250 km). However, there are no large-scale changes in this pattern in association with the physical transition.

We have simplified this strong interannual variability in the large-scale changes of pigment patterns at the time of the spring transition by decomposing the image composites into empirical orthogonal functions (EOFs). Each of the 15-day composites shown in Plate 1 was spatially averaged into 1° × 1° blocks (Figure 1) using only cloud-free pixels. This spatial averaging assigned a pigment concentration to more than 97% of the total number of blocks, with the remainder filled by spatial averaging of the blocks immediately to the north and south. The pigment pattern represented by the blocks (now 125 spatial points per field) were treated as a 10-point time series (the 15-day composites before and after the transition event in each of the 5 years) for calculation of the EOFs. Each mode of an EOF decomposition is composed of a spatial pattern whose amplitude in time is described by a time series. Actual pigment concentration associated with the mode for any spatial point at a particular time can be reconstructed by multiplication of the spatial value and the amplitude in the time series.

The spatial patterns and amplitude time series of the dominant modes of the EOFs of pigment patterns during the spring transition are shown in Figure 2. The first mode explains 60.1% of the total variance with a spatial pattern describing an offshore region of maximum change associated with the transition event (Figure 2*a*). The time series shows the strength of this pattern during the 15-day periods before and after the transition in each of the 5 years. This mode is dominated by the strong increase in offshore chlorophyll in 1980 (the time series indicates a positive change), with weaker offshore increases in 1981 and 1982. No similar change is seen during the 1983 and 1986 transition. The second EOF mode, accounting for 10.3% of the total variance, primarily represents variance north of ≈43°N where the CZCS algorithm is not reliable. This mode is not interpreted further. The third EOF mode (Figure 2*b*) explains 8.3% of the variance and although of questionable statistical significance, agrees well with, and helps quantify, the visual interpretation. This mode shows a region of maximum variance next to the coast between ≈36°N and 41°N. The time series shows both 1981 and 1982 to have positive changes (increases in pigment concentration) associated with this pattern, with 1981 having the largest response. This pattern did not change during the transition in 1980 and actually decreased in 1983 and 1986.

4.2. *Temporal Changes in Pigment Concentration*

To characterize the temporal development of changes in pigment concentration at the time of the spring transition, a time series of fourteen 10-day composites of the CZCS data was formed of the six 10-day periods before and eight 10-day periods after the event in each year. Each of these composites was spatially averaged into five 1° wide zones between 34°N and 41°N (see Figure 1) to provide an indication of cross-shelf variability in the temporal changes. This latitudinal range was where maximum interannual variability and maximum changes in pigment concentration were seen in the 15-day composites (Plate 1).

The time series of concentrations in each of the five zones in each year are shown in Figure 3, together with alongshore wind stress and the strength of the wind mixing for the same period. Wind forcing will be discussed in section 5. These pigment time series include images from the early portions of each year when the CZCS algorithm is known to produce artificially high values at higher latitudes. We have attempted to reduce this error by subtracting a correction function from the original images prior to the formation of the temporal and spatial averages. This function is latitudinally dependent (increasing from south to north) with a period of 1 year, maximum in winter and minimum in summer. We assume that the true chlorophyll levels are low some distance from the coast for most of the year. The function is obtained from an EOF analysis of 5 years of monthly averaged CZCS data images subsampled to form a 2.5° wide strip beginning 2.5° offshore, extending from 25°N to 50°N. Our assumption is that a latitudinally dependent function with an annual cycle and a peak at high latitudes in the winter months is primarily due to algorithm failure (dominated by Rayleigh scattering error) and not in situ biological processes in this offshore region. The first EOF mode (70.5% of the variance in this offshore strip) shows this latitudinal pattern and seasonal cycle. Interpolated values of this function, depending on latitude and date, were subtracted from the images used to form the time series presented in Figure 3. This correction function reduces pigment concentrations in the early parts of the times series (average reduction of 1.3 mg m^{-3} in February) but has little effect at the time of the transition and later into the year. In addition to the algorithm errors, any true annual cycle in offshore pigment with a winter maximum is also removed by the correction function. As this study is an analysis of relatively

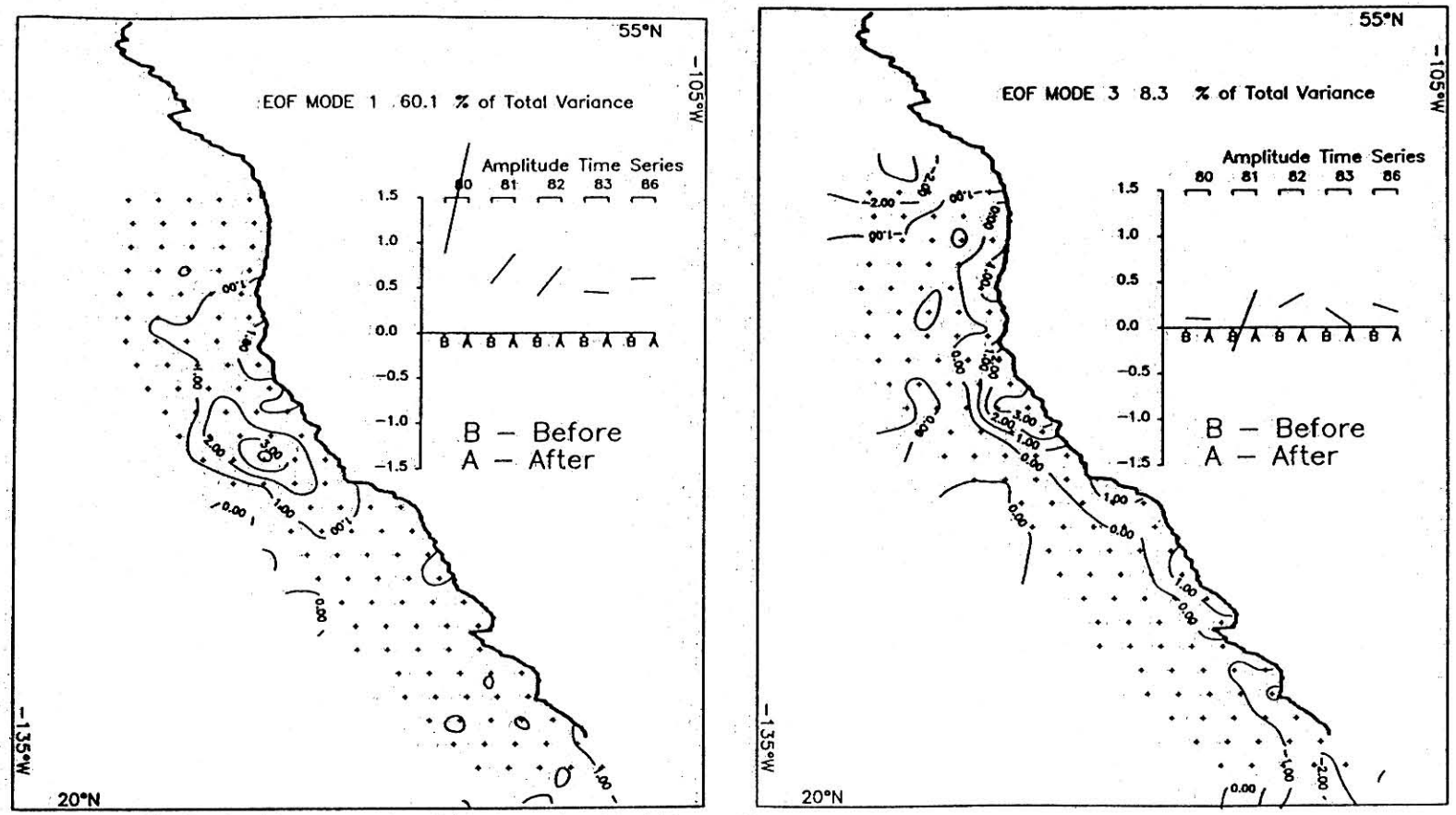

Fig. 2. Spatial patterns and amplitude time series of the (*a*) first and (*b*) third most dominant EOF modes of pigment patterns at the time of the spring transition. The time series shows the strength of the corresponding spatial pattern before and after the transition date in each of the years analyzed. The second mode (10.3% of the total variance) represented primarily variance north of ≈43°N where the CZCS algorithm is most suspect (see text).

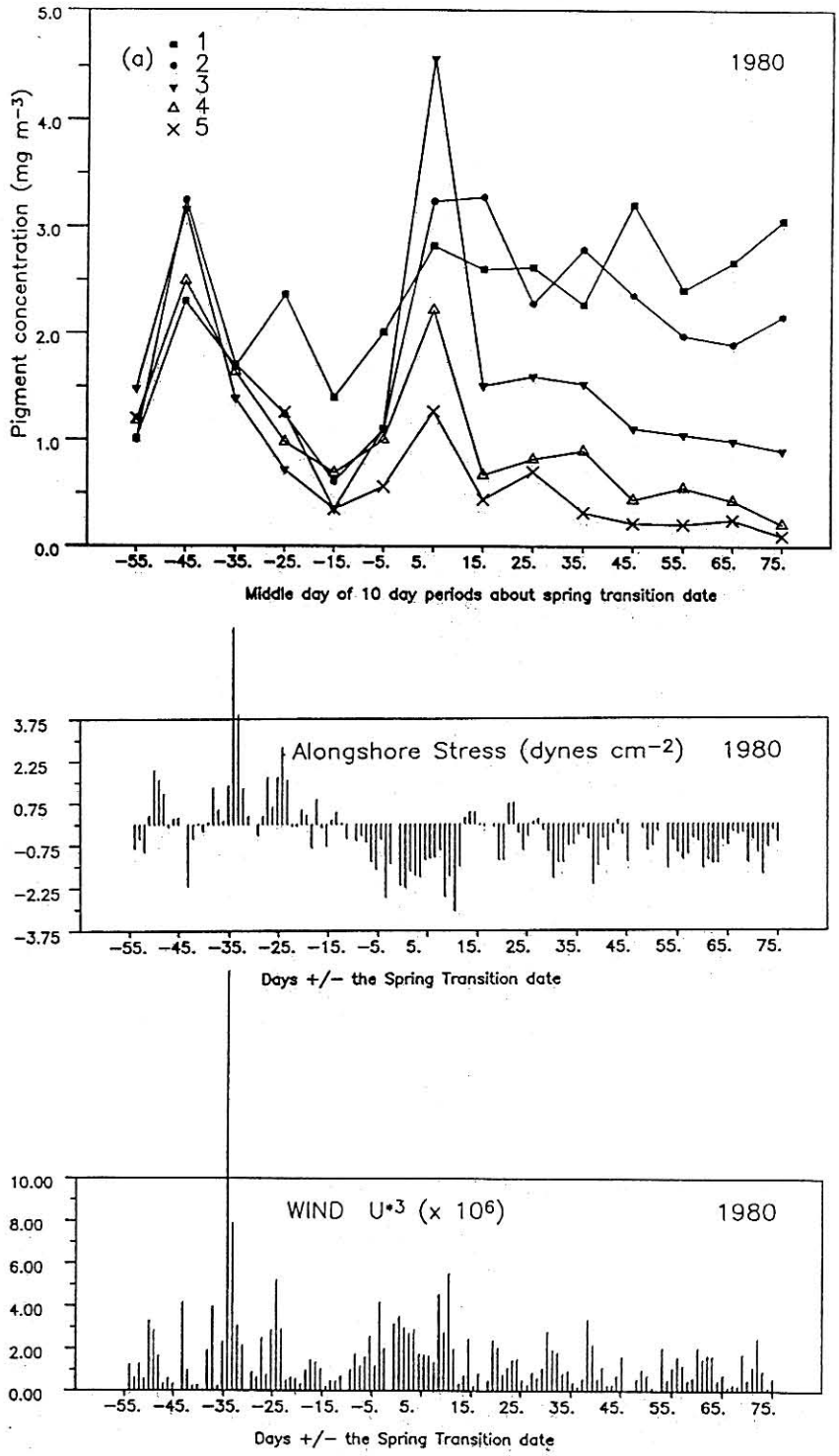

Fig. 3. Time series of pigment concentrations formed from 10-day composites spatially averaged over each of five 100-km-wide zones progressing offshore (zones 1–5 shown in Figure 1) for (*a*) 1980, (*b*) 1981, (*c*) 1982, (*d*) 1983, and (*e*) 1986. The spring transition date forms the starting point for six 10-day periods before and eight 10-day periods after the spring transition date for each year. Each time point represents a 10-day mean concentration and is plotted as the middle day of that period. Missing time points indicate that no satellite pigment estimates were available in the zone over the 10-day time period. Also shown for the same time period are daily values of alongshore wind stress and wind mixing strength (U_*^3) calculated from LFM wind data and averaged over all grid points within the five-zone region shown in Figure 1.

short time scale events superimposed on the annual cycle, the removal of any such annual cycle was not considered a problem.

The time series of pigment concentrations in each of the five zones during 1980 is shown in Figure 3*a*. These data show that the zone nearest the coast (zone 1) maintains a relatively high concentration (2.0–3.0 mg m^{-3}) both before and after the transition event. In the four zones farther from

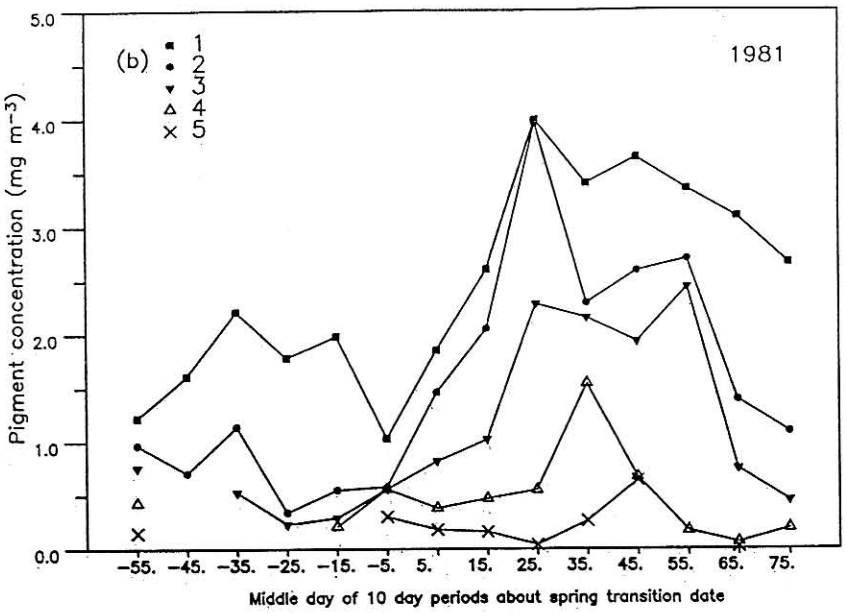

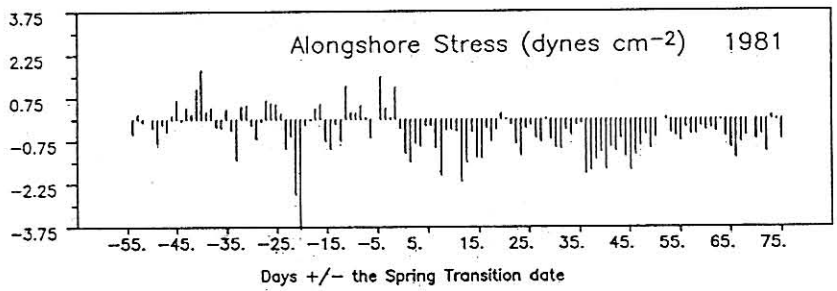

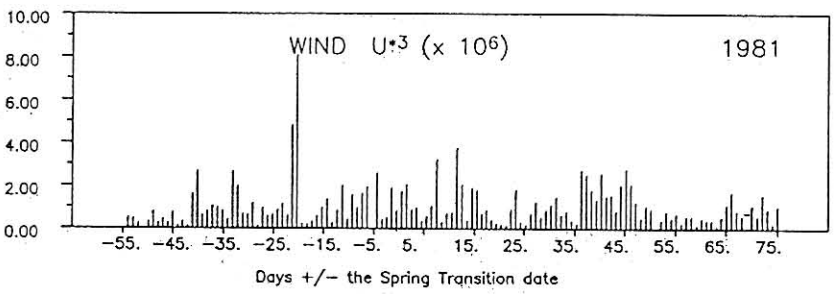

Fig. 3. (continued)

shore (zones 2–5), however, pigment concentrations increase sharply in the 10-day period (plotted as day 5) after the transition, to values 2–4 times higher than those immediately prior to the transition. These concentrations decrease after the first 10-day period, initially very rapidly but then return slowly to pre-transition concentrations after ≈50–60 days. The magnitude of the increase and the mean pigment concentration associated with this increase are greatest 200–400 km offshore.

The 1981 time series (Figure 3*b*) support the observation that the primary response of pigment concentrations to the transition in this year is in regions closest to the coast. Increases in mean pigment concentration begin at the time of the transition but increase more gradually than those in 1980. Increases are maximum within 200 km of the coast (zones 1 and 2) (from ≈1.0 mg m^{-3} to 4.0 mg m^{-3}), decreasing in magnitude in zones farther seaward. High concentrations are maintained over a month-long time period. Thereafter, con-

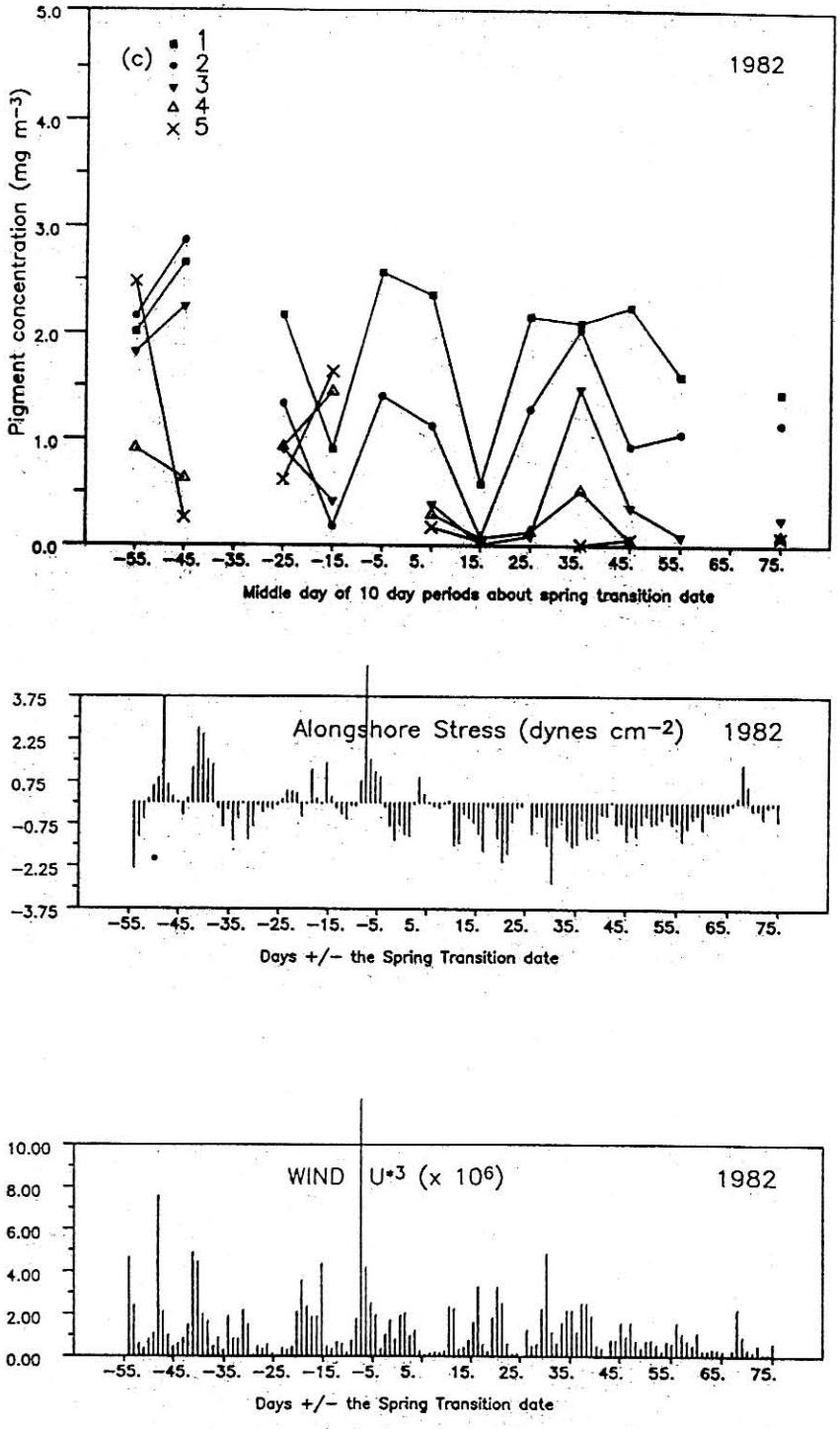

Fig. 3. (continued)

centrations appear to decrease. Concentrations in the three zones nearest the coast are higher after the transition than at any time prior to the event.

The pigment concentration time series in 1982 (Figure 3*c*) indicates a series of episodic events with largest amplitudes in zone 1 and decreasing amplitudes in zones farther from the coast. A short time scale increase (≈20 days) is initiated in the 10-day period immediately prior to the transition in the two zones closest to the coast, followed by a decrease to pretransition values and then another increase in the 30- to 40-day period after the transition. These data are difficult to interpret due to the gaps caused by clouds; however, changes in concentration in regions nearer the coast do appear more episodic in 1982 than in previous years.

In 1983 (Figure 3*d*) the largest increase in pigment concentration is dissociated from the date of the physical transition. There is a minor increase in concentration (0.5 mg m^{-3}) at the time of the physical transition that is restricted to the two zones nearest the coast (1 and 2) and of short (≈10 days) duration. The time series shows a relatively large concentration increase in the period 40–20 days before the transition (peaks of 4.5 and 3.2 mg m^{-3} in zones 1 and 2,

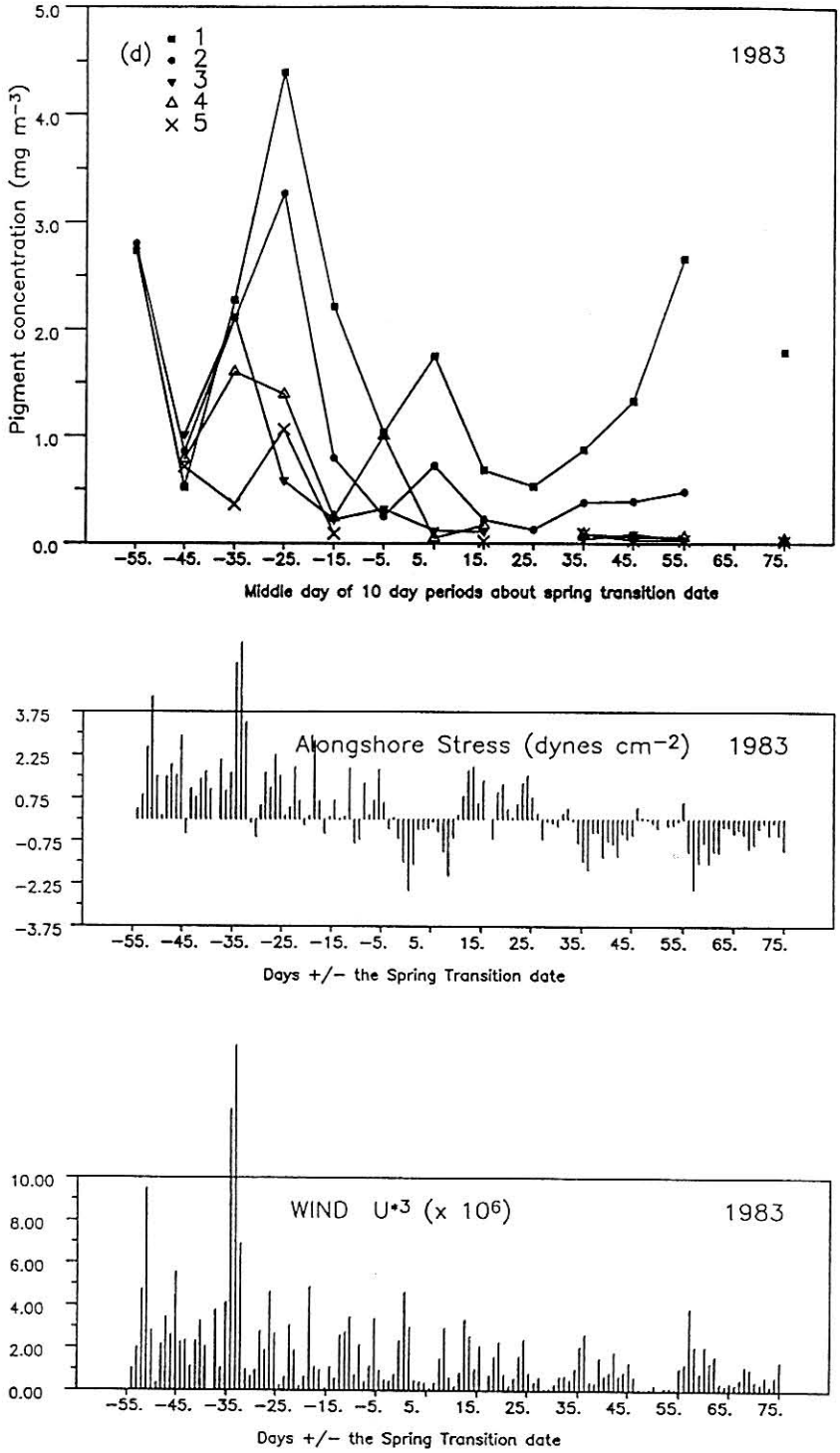

Fig. 3. (continued)

respectively) followed by a sharp decrease immediately prior to the transition (days 10–0). After the transition, fluctuations in concentration occur only within 100 km of the coast, and concentrations in all four zones to seaward remain low (<0.4 mg m^{-3}) in comparison to previous years.

Pigment concentrations in 1986 (Figure 3*e*) increase in the period 30–20 days prior to the transition date but exhibit relatively little variability after this. No major change occurs at the time of the physical transition. Increases associated with the transition event occur only in the two zones nearest the coast and are of short duration ($\approx$10 days) and small magnitude ($\approx$0.5 mg m^{-3}). A relatively stable cross-shelf concentration gradient is maintained throughout the study period with the three zones farthest seaward exhibiting only small changes in concentration.

The algorithms used to estimate pigment concentration from the satellite data assume that color in the water is derived from chlorophyll and related degradation products (case 1 water). Regions where significant amounts of color are contributed from other sources (case 2 water) will appear

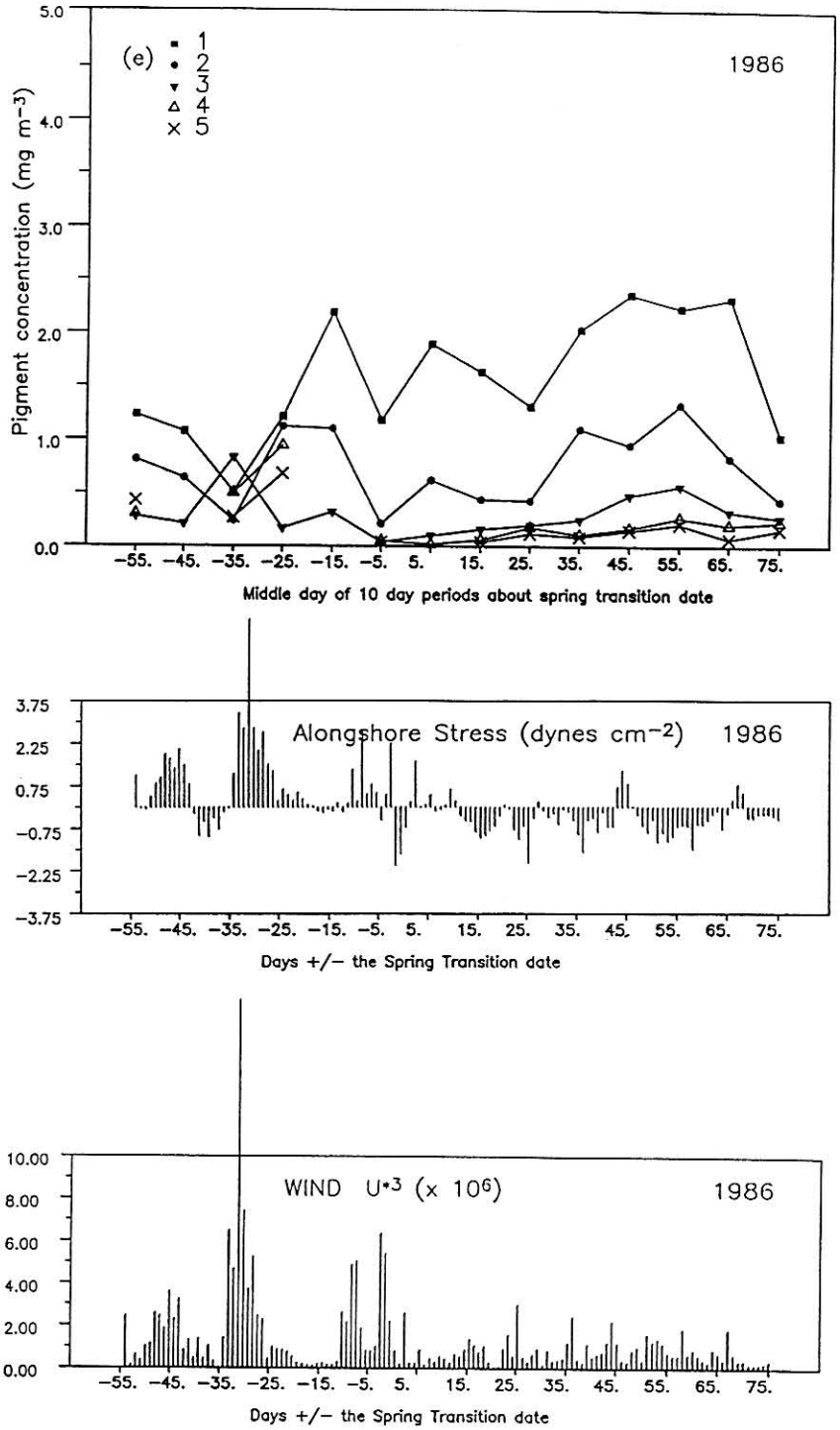

Fig. 3. (continued)

as regions of high pigment concentration in the imagery. This problem will be greatest near the coast over the shelf and probably contributes to the consistently high values observed closest to the coast where turbulence and runoff introduce sediment into the upper water column. In the study region, however, the shelf is usually of the order 20–30 km wide, and regions farther offshore are less likely to be turbid owing to suspended sediment. The fact that the zone closest to the coast in Figure 3 (zone 1) is an average over a 1° wide band reduces the potential bias introduced by shelf turbidity. Furthermore, the strong temporal correlation of pigment concentration between this zone and those further to seaward argues that concentrations averaged over zone 1 are not unduly contaminated by case 2 water.

5. Discussion

We have posed the question, What is the response of pigment concentration to the onset of upwelling favorable winds at the time of the spring transition? The results

presented in the preceding section demonstrate a large degree of interannual variability in the spatial pattern and temporal development of pigment concentrations at the time of the physical spring transition. The large increase in concentration in 1980 occurs offshore as a diffuse pattern over a large spatial area and does not appear to have been connected to coastal upwelling. The large increase in 1981 is more closely confined to the region near the coast, spreading offshore after the transition in a manner consistent with previous descriptions of a wind-driven coastal upwelling event. The response in 1982 is concentrated near the coast but is weaker and more variable in both space and time than that in previous years. In 1983 there is actually a decrease in pigment concentration at the time of the physical transition, but a major increase takes place 20–30 days prior to the transition. Concentrations in 1986 are higher than those in 1983, both before and after the transition, and extend farther from shore. However, there is little change in either concentration or pattern at the time of the physical transition. Instead, concentrations within 200 km of the coast increase in the period 20–30 days before the physical transition. The interannual variability of these responses does not appear to be directly related to the actual date of the physical transition per se (see Table 1). Neither the spatial patterns nor the time series of pigment concentrations show a consistent relationship to the Julian day of the event. Our discussion, then, is directed at identifying forcing mechanisms that can account for the interannual variability in the spatial pattern of pigment increase in those years when concentrations do show a response to the physical transition, and that can account for those years in which concentration increases were dissociated from the physical event.

Three possible mechanisms might account for the increases in pigment concentration in the spring. First, increases in concentration could be due to a localized increase in the rate of primary production. In a nutrient-limited regime, increases in production are dependant on a vertical and/or horizontal flux of nutrients. In a light-limited regime, a reduction in the depth of mixing (increased vertical stratification) and/or increases in solar radiation can lead to increases in rates of production. Second, offshore increases in chlorophyll biomass observed in the images after the transition might be a result of advection due to offshore Ekman transport and/or to coastal jets from nearshore zones of high productivity. The third possibility is that there is no increase in total water column pigment concentration but simply a vertical redistribution of existing phytoplankton within the water column. The CZCS integrates pigment concentration over one attenuation depth. An apparent increase in concentration will occur if vertical mixing brings an increased proportion of the total water column biomass within the upper attenuation depth. This depth-sampling bias of the CZCS also contributes (along with the atmospheric algorithm failure) to the apparently inverted seasonal cycle in chlorophyll biomass often observed in the satellite data [*Campbell and O'Reilly*, 1988; *Michaelson et al.*, 1988].

5.1. *Water Column Conditions in the Late Winter*

Unfortunately, there are virtually no in situ biological data during the time periods of interest describing the properties of the water column in the region where maximum interannual variability in pigment patterns occurs. Vertical profiles of hydrographic and biological properties from two CalCOFI line 60 stations (≈300 and 400 km off San Francisco) in February 1984 [*SIO*, 1984] are shown in Figure 4. These indicate a well-mixed surface layer extending to 75 m depth. Within this mixed layer, nitrate levels are low and uniform (0.2 μM) and chlorophyll levels are low (0.1–0.2 mg m^{-3}). The offshore profile indicates a deep chlorophyll maximum of ≈0.3 mg m^{-3}. Beneath the mixed layer is a strong pycnocline, coincident with the nutricline. CalCOFI data from regions closer to shore during the same survey show a somewhat shallower mixed layer (50 m); offshore data from farther south (line 77 at 33.4°N) during this survey show similar mixed layer depths and a coincident nutricline with higher temperatures, lower nitrate, and similar chlorophyll concentrations. Data from February 1985 [*SIO*, 1985] from line 80 (32.8°N) show similar conditions for this offshore region. Thus the profiles shown in Figure 4 are taken to represent upper ocean conditions prior to the transition in the offshore region of interest (zones 3–5 in Figure 1). Conditions closer to shore, where pigment concentrations generally remained relatively high, indicate a shallower mixed layer depth and nutricline. Most CalCOFI data during these cruises are from south of Point Conception where the satellite data show little response to the physical transition (Plate 1). The in situ data indicate that in these regions the nutricline is often below the pycnocline and probably remains relatively isolated from surface physical forcing. This may explain why the region of pigment increase seen at the time of the transition in 1980–1982 is not observed south of ≈33°N.

These CalCOFI data suggest that the water column sampling bias of the CZCS is not responsible for large-scale increases in pigment concentration observed in the image composites. The possibility that increases in concentration are due to a vertical redistribution of existing phytoplankton biomass presupposes the existence of a deep chlorophyll maximum of biomass sufficient to account for the ≈4 and 2 mg m^{-3} increases in concentration observed in 1980 and 1981 image composites, respectively, when integrated over the upper attenuation depth. While the vertical profiles shown in Figure 4 do indicate the presence of a deep chlorophyll maximum, the magnitude of this maximum would be insufficient to account for the observed increases if it were mixed vertically into the upper attenuation depth observed by the CZCS.

5.2. *Advection*

It is possible that advection of biomass from coastal upwelling regions contributes to the observed interannual variability in pigment pattern at the time of the transition. Water properties associated with an upwelling front can be carried into offshore regions by advection and eddy diffusion in areas of strong and persistent upwelling [*de Szoeke and Richman*, 1984]. Offshore Ekman transport is dependant on southward wind stress, which is linked to the forcing of the transition itself, becoming strong only after the spring transition date [see *Strub et al.*, 1987*a*]. Time series of daily alongshore wind stress (spatially averaged over all five zones shown in Figure 1) are presented in Figure 3 and show that the transition date in each year is associated with a southward wind event. This event is strongest in 1980 and most

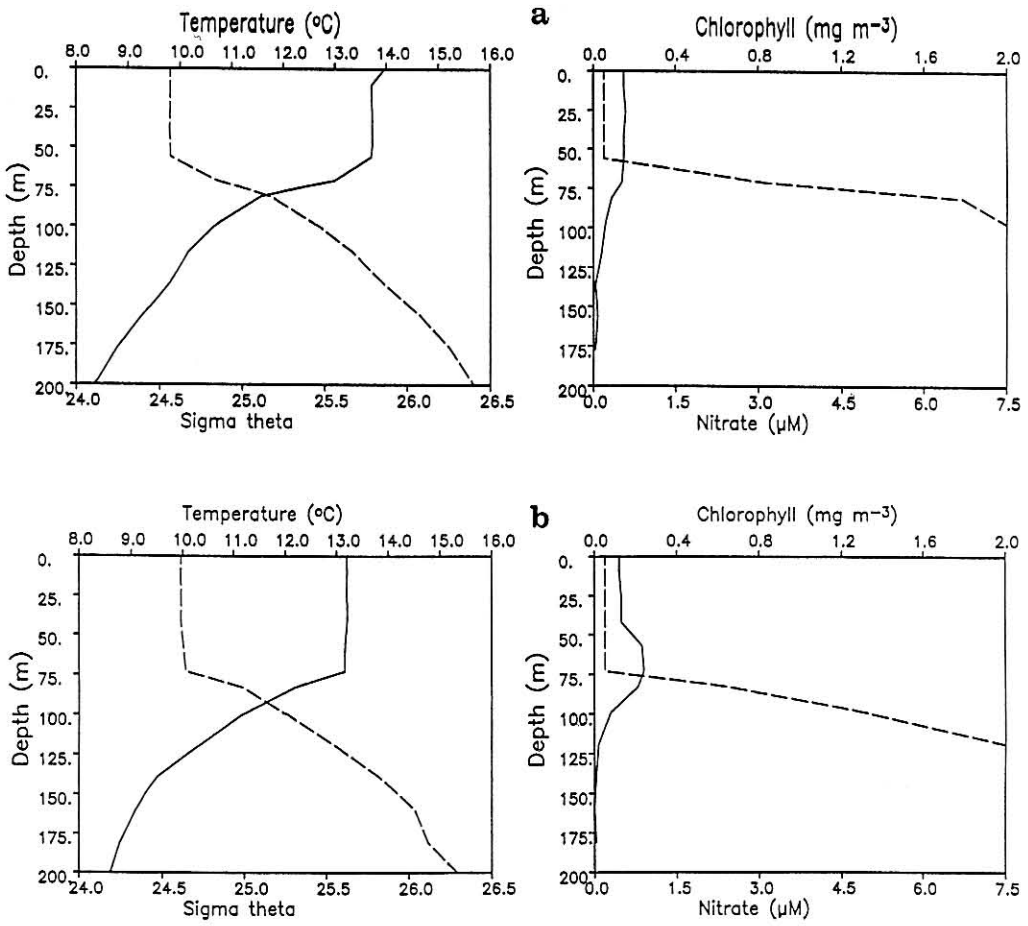

Fig. 4. Representative vertical profiles of temperature, density, chlorophyll concentration, and nitrate concentration in the pretransition period for the offshore region of maximum pigment concentration variability (see Plate 1): (*a*) CalCOFI station 60/90 (36°36.2′N, 125°47.7′W) and (*b*) CalCOFI station 60/100 (36°16.5′N, 126°29.4′W), in February 1984. The stations are approximately 305 km and 380 km offshore, respectively. Density and nitrate concentration are shown by the dashed profiles in the right and left plots, respectively.

persistent in 1981. It is least persistent in 1982 and 1986, when periods of northward wind stress (relaxation of upwelling) occur within 5 days after the transition date. Ekman transport velocities in the surface layer measured by *Kosro* [1987] during an upwelling event off northern California were of the order of 5.0 cm s^{-1}. At this velocity, phytoplankton supported by coastal upwelling would take ≈70 days to be advected 300 km offshore. Advection from upwelling zones is thus unable to explain the sudden offshore increase within 10 days of the transition date in 1980 (Figure 3*a*); nor does it explain increases in concentration that occur prior to the transition date during periods of northward wind stress in other years. The temporal trend in 1981 (Figure 3*b*), however, is more consistent with patterns expected during coastal upwelling and offshore advection. Major increases in concentration occur after the onset of southward wind stress and are more closely associated with the coast than those in 1980. Maximum concentrations do not occur until 20–30 days after the transition, occurring first in zones closer to shore and later in zones farther from shore.

Cross-shelf jets off the California coast [*Mooers and Robinson*, 1984; *Abbott and Zion*, 1987] have cross-shelf velocities exceeding 50 cm s^{-1} [*Mooers and Robinson*, 1984; *Kosro*, 1987] which could advect biomass 300 km offshore within a 7-day period. The spatial patterns of pigment in 1980 do not suggest such features. The large scale and diffuse pattern of increased concentration and the lack of any visual evidence of jets in individual images making up the composite suggest that jets were not responsible for high offshore pigment concentrations in 1980. This argument appears less valid in 1982, when surface pigment patterns after the transition resemble jets previously seen in satellite images [*Rienecker et al.*, 1985; *Abbott and Zion*, 1987].

Advection of biomass from coastal upwelling sites does not explain all of the observed interannual variability in either the magnitude of the pigment changes or the spatial pattern of observed increases. While advection may play a role in the observed pigment distributions, it does not explain the large and diffuse increase 300–500 km offshore in 1980, nor does it explain the pretransition increases in 1983 and 1982 following strong northward winds associated with downwelling and onshore Ekman transport. Furthermore, Figure 3*d* shows that upwelling-favorable (and offshore transporting) winds were present in 1983 when no changes in concentration took place at the time of the physical transition.

5.3. *Quantification of the Light Regime*

Low concentrations of nitrate (<0.2 μM) in the upper mixed layer and a subsurface chlorophyll maximum (Figure

TABLE 2. The Spring Light Regime

Year	Day When Solar Radiation Exceeded 157 W m^{-2}		15-Day Mean, W m^{-2} (34°N to 41°N)	
	Date	Days Relative to ST	Before ST	After ST
1980	March 14	−6	181	203
1981	March 25	−1	154	239
1982	March 20	−30	205	260
1983	March 31	−5	174	235
1986	March 16	−1	142	191

ST, spring transition.

4) suggest that light is not limiting in this region of the CCS in winter. This argues that observed pigment increases in the spring do not develop in response to the classical North Atlantic spring bloom situation parameterized by *Sverdrup* [1953]. We test this assumption using the quantification of *Riley* [1957], who shows that depth-averaged, vertically integrated solar radiation in the upper mixed layer must be greater than ≈43 Ly d^{-1} for the spring bloom to start in the North Atlantic (assuming nutrients are not limiting). Using an extinction coefficient of 0.1 m^{-1} and the mixed layer depth of 75 m indicated in Figure 4, we integrate and solve the light extinction equation $I_z = I_0 e^{-kz}$ for I_0. With this model, an I_0 of 157 W m^{-2} is necessary to initiate a spring bloom. Total incident clear sky solar radiation can be modeled as a harmonic function of latitude and Julian day [*Reed*, 1977]. Solar radiation values for 39°N were calculated and modified by the mean observed daily cloud cover obtained from the COADS data set and compared with this 157 W m^{-2} value. Details of the solar radiation model and modification for cloud cover are given in Appendix A.

Table 2 shows the dates in each year when the spatially averaged (over a region approximating zones 1 and 2 in Figure 1) solar radiation exceeds 157 W m^{-2} as well as the mean solar radiation for the 15-day periods before and after the spring transition date in each year. Except for 1982, the date when a North Atlantic type of spring bloom situation could develop is closely associated with the date of the transition and does not explain the large differences in pigment response in 1980 and 1981 compared with 1983 and 1986. The mean light intensity over the 15-day periods before and after the transition dates indicate that light is probably not limiting either before or after the transition, except in 1986. Again, these data cannot explain the large interannual differences in pigment response to the spring transition and substantiate the argument that light is not limiting during the late winter and spring in this region of the CCS. Note especially that the major increases in pigment concentration in 1983 and 1986 occur a month prior to the earliest physical transitions when light levels are low.

5.4. *Wind Forcing*

Vertical profiles of nitrate and chlorophyll from this region of the CCS in winter (Figure 4) suggest that the surface mixed layer is a nutrient limited regime. Differences in wind forcing and resulting vertical nutrient flux to the upper part of the water column might be responsible for the observed interannual variability in pigment concentrations during the physical spring transition. This forcing can be either vertical mixing by the wind or upwelling due to southward alongshore wind stress, both of which might introduce nutrients into the upper water column. Conversely, vertical transport of nutrients is affected by the water column density structure (mixed layer depth and stratification), its position relative to the nutricline, surface heating at the time of wind events, and the relative depth of previous mixing events. The vertical profiles shown in Figure 4 (and other data from this and 1985 CalCOFI cruises) indicate that for pretransition periods in 1984 and 1985, the areas of maximum pigment variability seen in Plate 1 (the offshore region north of ≈34°N) are regions where the nutricline is coincident with the pycnocline. In such regions, surface forcing can significantly affect the flux of nutrients into the upper water column.

Daily values of both wind mixing strength (as u_*^3) and alongshore wind stress are plotted in Figure 3 for the same time period as the pigment time series. These data show that increases in pigment concentration prior to the transition date occur following strong wind mixing events. After the transition dates, strong wind mixing events are also upwelling events, and it is not possible to separate their respective effects. We present daily values of the wind products rather than temporal means in order to show the peaks in wind forcing.

The short time scale pigment increase at the transition date in 1980 (Figure 3*a*) is associated with a sustained period of increased mixing which starts approximately 5 days prior to the transition date. This wind is also upwelling favorable and results in the largest pigment increase observed at the time of the transition in the image composites. Nutrient flux into the upper water column due to the combined effect of wind-driven vertical mixing and upwelling can explain the simultaneous increase in concentration in each of the zones as well as the large and diffuse pattern of these high concentrations seen in Plate 1*a*. The reason why the strong mixing event 35 days prior to the transition is not associated with an increase in pigment concentration is not evident in these data. The event, however, is of short duration (2 days) and occurs sufficiently early in the year (mid February) for light levels to be very low.

In general, no large wind mixing event takes place prior to the transition in 1981 (Figure 3*b*). The post-transition increase in pigment concentration occurs in association with the southward alongshore wind stress which begins at the transition date. Both the previously discussed spatial patterns and time series suggest that 1981 pigment concentrations are responding to a wind-driven coastal upwelling event and subsequent offshore advection. A moderate, short

TABLE 3. The Mean Wind Regime for 15-Day Periods Before and After the Spring Transition Averaged Over the Region 34°N to 41°N

	Alongshore Wind Stress, dyn cm^{-2}		Wind Mixing U_*^3, $\times 10^{-6}$	
Year	Before	After	Before	After
1980	−0.105	−0.120	1.8	2.2
1981	0.015	−0.100	1.3	1.4
1982	0.024	−0.040	2.1	0.9
1983	−0.002	−0.004	1.8	1.3
1986	0.026	−0.094	2.3	0.7

time scale mixing event which is also upwelling favorable takes place 20 days prior to the transition and might be associated with slight increases seen in the two zones nearest the coast in the period 10–20 days before the transition.

The increase in 1982 which begins in the 10-day time period just prior to the transition is associated with a strong mixing event during northward winds beginning at day −8 (Figure 3*c*). A second increase in the three zones closest to shore 20–40 days after the transition is associated with southward wind stress beginning at day 20.

The pigment time series in 1983 shows that the major increase in concentration 20–40 days prior to the transition is associated with large values of u_*^3 beginning at day −37 (the end of February) (Figure 3*d*). Although wind mixing remains relatively strong during the actual transition, an increase in concentration takes place only in the zone closest to the coast at this time. This increase is relatively minor and is associated with a 2-week period of southward wind stress. Concentrations in all four zones farther seaward remain low after the transition despite this southward wind stress. It is possible that the lack of pigment response to wind mixing and southward alongshore wind stress (upwelling) after March in 1983 is due to an anomalously deep pycnocline and nutricline associated with the 1982–1983 El Niño. A deeper pycnocline would increase the isolation of surface water from deeper, nutrient-rich water. *Rienecker and Mooers* [1986] show the surface mixed layer off northern California in February 1983 to be warmer, deeper, and more strongly stratified than the climatological mean. *Huyer and Smith* [1985] show the April 1983 pycnocline off Oregon to be ≈40 m deeper than a 6-year average, and McGowan [1985] shows the March nutricline off southern California to be at 80 m compared with the usual 50 m.

Pigment concentrations in 1986 in the two zones closest to the coast increase in the period 20–30 days prior to the transition in association with a strong wind-mixing event beginning at day −34 (Figure 3*e*). The data show that these winds would not induce upwelling. Concentrations remain relatively constant after this period, potentially supported by another strong mixing event and the onset of southward alongshore wind stress at the time of the transition. Increases in concentration in the second and third zones from the coast, beginning 30 and 40 days (respectively) after the onset of upwelling are consistent with offshore advection of pigment.

We have summarized the interannual variability of surface wind forcing by forming spatial averages of u_*^3 and alongshore wind stress over the entire five-zone region shown in Figure 1 for the 15-day periods before and after the transition event in each year. Table 3 shows that 1980 has the strongest upwelling favorable winds and is the only year in which they were present both before and after the transition. In addition, wind mixing is relatively strong both before and after the transition. In 1981, wind mixing is weaker, but southward wind stress becomes strong after the transition. It is interesting to note that 1980 and 1981, the only years with a strong increase in pigment concentration at the transition, are also the only years with stronger wind mixing after the transition than before. In both 1982 and 1986, wind mixing becomes weak after the transition. Strong mixing before the transition in 1986 is accompanied by relatively strong southward wind stress after the transition to maintain approximately constant concentrations over the transition period. The inability of relatively strong wind mixing at the time of the transition in 1983 to introduce nutrients into the upper water column might be due to the anomalously deep pycnocline.

For the late winter and early spring periods analyzed in this study, the curl of the wind stress does not appear to play a strong role in nutrient input to the upper water column. Previous work [*Chelton*, 1982] suggests that offshore regions of increased zooplankton biomass in the southern CCS during summer might be an indirect response to nutrient input by Ekman pumping associated with a zone of positive wind stress curl. Comparison of the contours of wind stress curl averaged over the 15-day periods before and after the transition date in each year show that the region of positive curl evident in climatological data [*Nelson*, 1977] expands offshore after the transition between ≈33° and 41°N. This response is strongest in 1980 and 1981 and weakest in 1986. However, maximum vertical velocities calculated from the wind stress curl are ≈0.3 m d^{-1}. Figure 4 shows the pycnocline (and nutricline) to be ≈75 m deep. These velocities are probably incapable of changing the nutrient regime in the upper attenuation depth of the water column sampled by the CZCS within the short (10–15 days) time period observed in Plate 1 and Figure 3. Furthermore, time series of wind stress curl over the same periods shown in Figure 3 show that the pretransition pigment concentration increases both in 1983 and 1986 are associated with time periods of generally negative curl.

5.5. *Model Evaluation of Interannual Variability in Vertical Mixing*

The preceding section discusses surface wind forcing as an index of offshore vertical mixing and coastal upwelling. Vertical mixing (in the absence of upwelling), however, is affected by a number of processes besides wind stirring (u_*^3). The effects of surface heating, penetrative radiation, and vertical shear of the horizontal currents at the base of the mixed layer are also important, as are the initial depth of the mixed layer and the strength of the stratification at the base of the mixed layer [*Niiler and Kraus*, 1977]. The lack of in situ density data from most years, however, prevents us from evaluating interannual differences in the density fields, except for the comments on the anomalously deep pycnocline during spring of 1983 noted above. Using a one-dimensional numerical model of vertical mixing, however, we can quantify the interannual variability in mixing caused

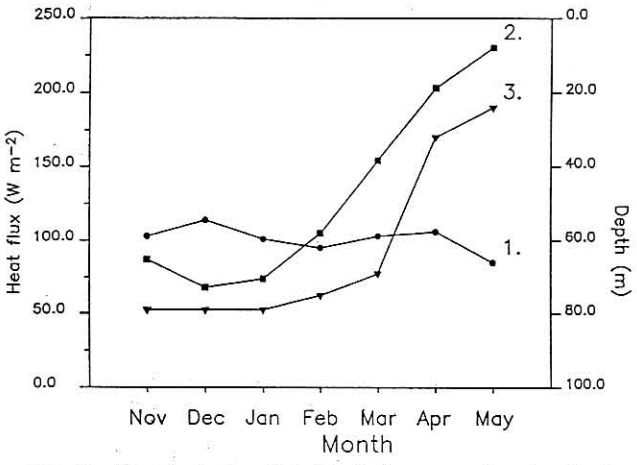

Fig. 5. Changes in the climatological mean surface heat budget terms in the winter and spring averaged over the region 34.5°–41.5°N and 121.5°–127.5°W showing cooling due to sensible heat flux + latent heat flux + net longwave radiation (plotted as circles, line 1) and heating due to solar radiation I_0 (squares, line 2). The depth of the mixed layer after 15 days of wind forcing by idealized wind stress under these conditions in each month is also shown (triangles, line 3).

by differences in wind stress and solar radiation. All of these processes are included in the model to some extent.

Components of the climatological monthly mean surface heat budget over the CCS are available from *Nelson and Husby* [1983]. These have been averaged over the region from 34.5°–41.5°N and 121.5°–127.5°W (excluding land) and are presented in Figure 5. They show the rapid increase in solar heating in March, while cooling due to all other terms remains nearly constant at $\approx$100 W m^{-2}. The degree to which surface winds can mix nutrients upward at the base of the mixed layer will depend on the timing of the wind events relative to this onset of net surface heating. Because a relatively cloud-free period of high radiation often occurs at the time of the transition, wind events associated with earlier winter storms should be more effective in mixing than the actual wind event associated with the transition and the onset of southward winds. Similarly, transitions that occur later in the season should be associated with less vertical mixing, owing to increased solar radiation.

Daily surface radiation estimated from COADS cloud cover and bulk radiation formulae (Appendix A) are used with twice-daily LFM winds to drive the one-dimensional second-order closure turbulence model of *Mellor and Yamada* [1982] for the period surrounding the spring transition in each of the 5 years considered above. Initial conditions for the model simulation of each year are identical and similar to those shown for the offshore profile of Figure 4 (75-m-deep mixed layer, started from rest). Details of the model are presented in Appendix B. The model is used as a measure of the relative differences in mixing power which result from the balance of wind and radiative forcing in each year, rather than as an absolute measure of mixed layer depths. Although less satisfying than actual in situ data, the model provides a mechanism for evaluating these competing influences on vertical mixing. Simpler scaling arguments for mixed layer depth based on daily or longer means of wind forcing, radiation, and heating [*Niiler and Kraus*, 1977; *Price et al.*, 1986] were evaluated and found to be less satisfactory, since these arguments apply to periods of constant forcing. The actual surface forcing in spring fluctuates between strong heating and cooling, as well as between stronger and weaker mixing, with diurnal and synoptic periodicity. The numerical model provides the means of quantifying the net effect of the competing, temporally varying, forces.

The model is first used as an alternate to simple scaling arguments to calculate the monthly mean mixed layer depths that might be expected from climatological forcing. Surface winds characteristic of typical winter storms are used in competition with climatological surface heating and solar radiation. These winds are typical of moderately strong mid-latitude storms with wind stress alternating between mildly southeastward (0.14 N m^{-2}) and strongly northeastward (0.32 N m^{-2}) with a 4-day period. Daily averaged solar radiation for each month is taken from *Nelson and Husby* [1983] and distributed over a cosine-shaped function with a 12-hour period followed by 12 hours of darkness to simulate the diurnal cycle. Surface cooling by processes other than solar radiation is held constant at 110 W m^{-2}. The model is run for 15-day period for each month and the maximum mixed layer depth (as defined by the density difference at the bottom of the mixed layer) over the last 4 days noted. This idealized seasonal progression of mean mixed layer depth and the surface forcing is presented in Figure 5. The results show that such winds would slightly deepen the initial 75-m mixed layer in November–January, maintain the mixed layer at 75 m depth in February, and result in mixed layer depths of 69, 32, and 24 m for the radiation typical of March, April, and May, respectively. This quantifies the notion that increasing solar radiation will inhibit vertical mixing as the season progresses.

Using the same initial conditions, the model is forced with the actual daily solar radiation and twice daily wind stress from each of the 5 years and constant net surface cooling (representing sensible and latent heat loss plus net infrared radiation). The solar radiation calculated from the harmonic bulk formula and cloud correction is greater than the climatological values presented by Nelson and Husby. To compensate for this, a greater net cooling of 130 W m^{-2} is used to avoid unrealistic heat buildup. Wind stress is increased by 50% to compensate for the known tendency of the Mellor-Yamada model to mix less than field measurements [*Martin*, 1985]. This is equivalent to increasing the drag coefficient used in the wind stress calculation from 1.3×10^{-3} to 2.0×10^{-3}. As the model results are interpreted in a relative rather than absolute sense, these modifications have no impact on our discussion of interannual differences.

Results of the model are shown in Figure 6 over the 15-day periods before and after the spring transition in each year. These results are presented as depth-time contours of the log (base 10) of the eddy diffusivity for heat, K_H, which also applies to other passive substances (including nutrients). In addition to eddy diffusivity, the model includes a constant background diffusivity of 10^{-5} m^2 s^{-1}. Thus, contours of -5 are taken to represent the bottom of the mixed layer, where the diffusivity begins to be governed by the background level of mixing rather than by turbulence. Regions of strong turbulent mixing ($K_H > 10^{-2}$ and $K_H > 10^{-1}$) are shown by hatching. In each year, there is an initial period of adjustment in the model usually lasting less than 2 days (several inertial periods). This is caused by using the same initial conditions in each year (the 1984 CalCOFI data) which are not in balance with the actual winds, radiation, heat flux and model dynamics of each year. Adjustment results in the

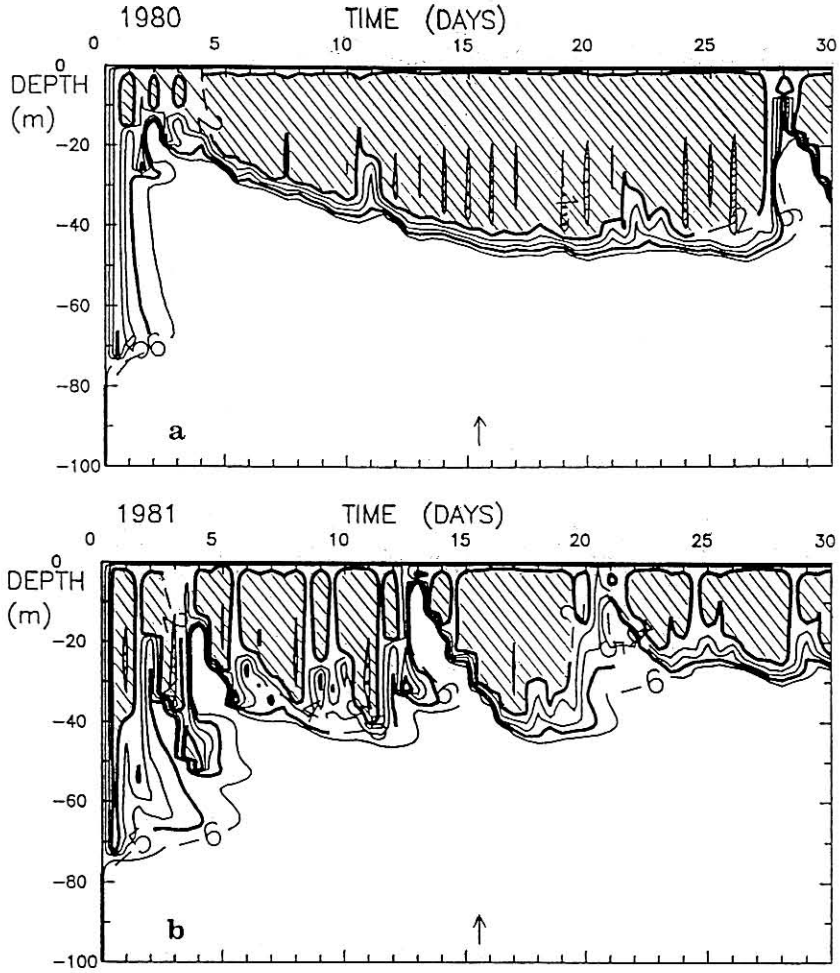

Fig. 6. Time-depth contours of $\log_{10}$ eddy diffusivity of heat, K_H, illustrating interannual differences in the mixing regime for the 30-day period starting 15 days before the spring transition date (shown as an arrow) in (*a*) 1980, (*b*) 1981, (*c*) 1982, (*d*) 1983, and (*e*) 1986. Diffusivity values were generated by a one-dimensional mixing model that balances daily wind stress and daily heat budget values. Periods of strong mixing ($K_H > -2$ and $K_H > -1$) are shown as hatched and cross hatched, respectively. The -5 contour, which equals the background diffusivity in the model, represents the extent of turbulence and is taken as the base of the mixed layer.

setup of stratification shallower than the initial 75 m in each year (mean conditions result in net heating of the water column prior to the transition in each year). It should be emphasized that the model is used to test the degree to which wind mixing, in the absence of upwelling, would bring nutrients into the upper water column.

Most years have a period of moderate to strong mixing prior to the transition due to winter storms (Figure 6). In 1982, 1983, and 1986, both the mixing intensity and mixed layer depth are strongly reduced after the transition. These are years with weak or nonexistent increases in offshore chlorophyll content at the time of the transition. In 1981 there is a 5-day period of mixing after the transition that equals the mixing prior to the transition. This year had the second largest posttransition increase in offshore chlorophyll concentration. In 1980, the feature that stands out as qualitatively different from the other years is the steady increase in mixed layer depth and mixing intensity. This is caused both by the increasing wind (Figure 3*a*) and by the lack of a strong increase in solar radiation at the time of the transition. These characteristics of the mixing regime would allow the steady erosion of the density gradient beneath the mixed layer and a continuous entrainment of nutrients over a period of 20 days or more. This steady increase in mixing intensity and entrainment over the 1980 transition period is not seen in other years and may explain the large increase in offshore pigment concentration evident in the satellite imagery shown in Plate 1*a*. In 1983 the pycnocline is known to have been deeper than the climatological mean, making the initial mixed layer used here too shallow and reducing the effect of mixing beyond that predicted by the model. The deepest and most intense mixing predicted by the model is seen 5–10 days prior to the transition in 1986 but does not appear coincident with any increase in pigment concentration. In this year, however, a stronger wind event occurs 25–35 days prior to the transition which is coincident with an increase in pigment concentration (Figure 3*e*). It is possible that the mixing event shown in the model either acts only to maintain the already elevated pigment concentrations by further vertical mixing or does not mix below the depth of the previous (and stronger) wind event, in which case, this mixing event does not introduce any new nutrients and need not be associated with an increase in pigment concentration. This is similar to the strong mixing and pigment response

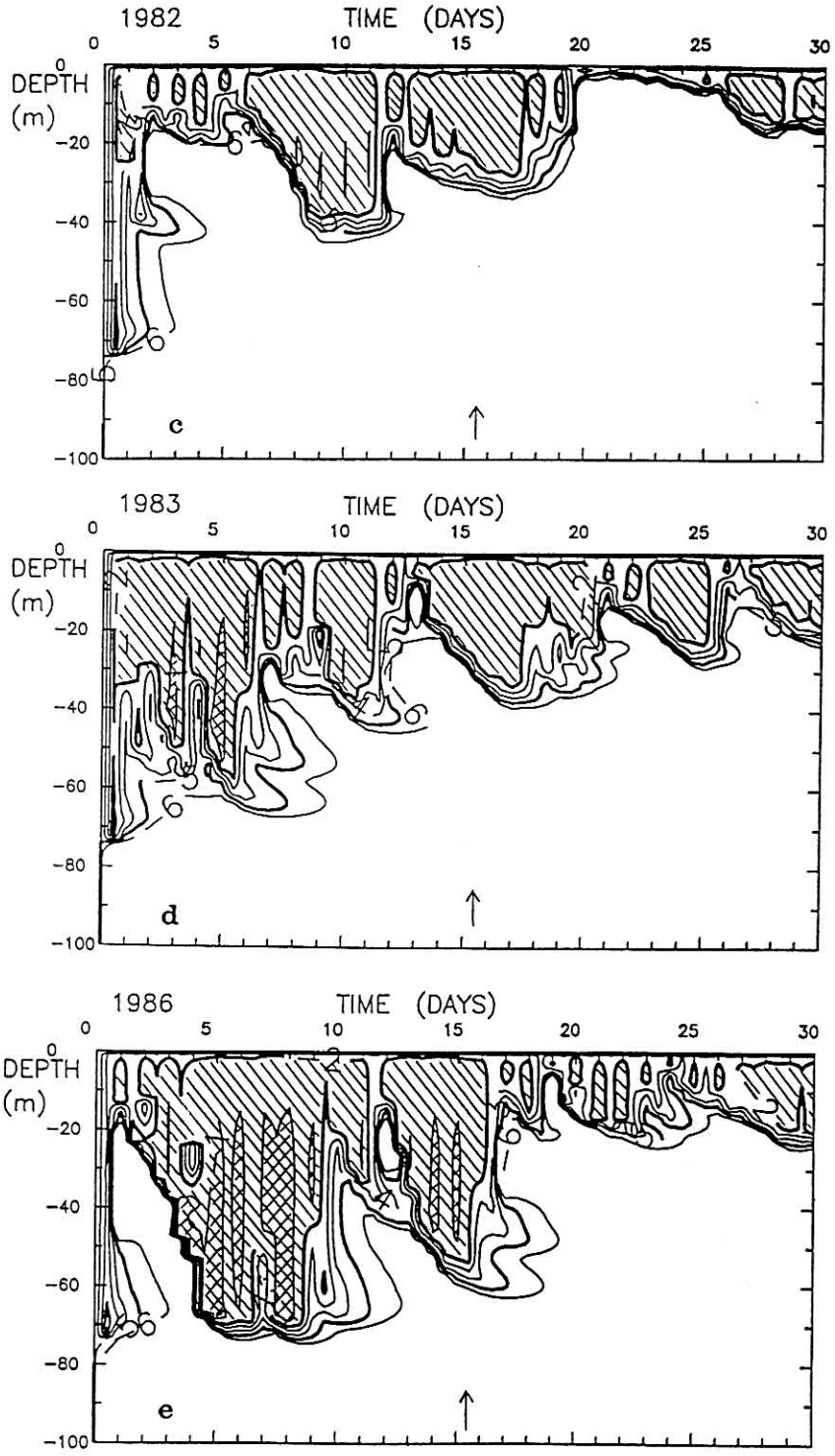

Fig. 6. (continued)

seen 35 days prior to, but not coincident with, the transition in 1983. These years illustrate the importance of the timing of the transition in relation to prior mixing events in late winter. Strong late winter wind events can reduce the role of wind mixing in the nutrient input at the actual time of the transition and make nutrient flux into surface layers a stronger function of alongshore wind stress and upwelling.

6. Summary and Conclusions

1. CZCS image composites reveal strong interannual variability in the changes in pigment pattern associated with the spring transition in current structure along the west coast of North America. In both 1980 and 1981, large increases in concentration take place between ≈33°N and ≈41°N. The

maximum increase in 1980 occurs in a region centered ≈300 km offshore, and in 1981 it occurs within 300 km of the shore. The magnitude of changes at the time of the transition is less in 1982, and spatial patterns of concentration more variable than those of other years. In both 1983 and 1986, virtually no change in pigment pattern or concentration takes place at the time of the transition.

2. South of ≈33°N, where the magnitude of the spring transition in wind and current structure is known to be small or nonexistent, changes in pigment concentration are also small in each of the years analyzed.

3. Pigment concentrations within 50 km of the coast over the entire study region (22°N to ≈41°N) remain approximately the same over the transition period, most likely owing to nutrient enrichment which occurs even in winter in shelf and coastal regions.

4. Time series of pigment concentration for extended periods before and after the transition show that the concentration increase in 1980 occurs within the 10-day period immediately after the transition date. In 1981 a more gradual increase over a 30-day period is initiated at the time of the transition. Temporal patterns in 1982 indicate episodic pigment increases in the zones within 200 km of the coast. Although no significant increase takes place at the time of the transition in either 1983 or 1986, relatively large increases do take place in the periods 20–40 days prior to the transition.

5. Available in situ data suggest that this region has a mixed layer ≈75 m deep and is strongly stratified and nutrient limited even in mid to late winter. Comparisons of CZCS measured pigment time series with wind forcing in each year show that increases both prior to and at the time of the transition are associated with strong wind mixing events. Beginning at the time of the physical transition, this wind mixing also represents southward alongshore wind stress (upwelling). Both of these processes support a vertical nutrient flux and potential increases in phytoplankton concentration. Interannual variability of this forcing in conjunction with variability in nutricline and pycnocline depths is most likely responsible for the observed interannual variability of pigment concentrations at the time of the transition.

6. Comparisons of the offshore wind-mixing regimes from each year are made with a one-dimensional mixing model. The model shows that strong vertical mixing in 1980 steadily entrains increasingly deeper water around the time of the transition. This might explain the large and diffuse offshore increase in pigment concentration in this year. Vertical mixing is also relatively strong in 1981 both before and after the transition date, with steady southward alongshore wind stress beginning at the transition date. The model shows that vertical mixing after the transition is relatively weak in each of the other years. Nutrient flux resulting from southward wind stress at the time of the transition in 1983 might also be reduced by the anomalously deep pycnocline (and nutricline) associated with the 1982–1983 El Niño.

7. These data suggest that surface pigment increases in the winter nutrient limited regime off central and northern California are strongly influenced by nutrient flux induced by wind forcing. In the early portion of the year, when solar heating is low, wind mixing is important. As the season progresses, the effect of wind mixing is reduced by stratification, and vertical nutrient flux is increasingly dependent on southward alongshore wind stress and resultant upwelling. This wind forcing is initiated at the time of the spring transition. Large increases in pigment concentration occur when both types of forcing occur together.

8. A large portion of the observed interannual variability in the response of pigment concentration to the spring transition (the onset of upwelling-favorable winds) appears to be due to the relative timing of this event with respect to prior wind mixing events and seasonal solar heating and stratification.

9. The results shown here demonstrate the danger of forming conclusions about spatial patterns based on just a few years of satellite data. It is obvious that our conclusions about the response of pigment concentration to the physical spring transition would have been very different had our analysis been restricted to the first 1–2 years.

APPENDIX A: SOLAR RADIATION FORMULAE

Incoming clear sky radiation was calculated from the harmonic formula of *Seckel and Beaudry* [1973]. This reproduces the values of the Smithsonian tables with an atmospheric transmissivity of 0.7. *Reed* [1977] found this formula to compare favorably with direct measurements over a range of latitudes extending from the Gulf of Alaska to the tropics. This formula is

$$I_c = A_0 + A_1 \cos(\phi) + B_1 \sin(\phi) + A_2 \cos(2\phi) + B_2 \sin(2\phi) \quad \text{(A1}a\text{)}$$

where I_c is the incident clear sky radiation, $\phi = 2\pi/365(t - 21)$, t is the Julian day number, and the other constants are functions of latitude λ, expressed in degrees:

$$A_0 = -32.65 + 674.76 \cos\left(\frac{2\pi}{360}\lambda\right) \quad \text{(A1}b\text{)}$$

$$A_1 = 19.88 + 397.26 \cos\left[\frac{2\pi}{360}(\lambda + 90)\right] \quad \text{(A1}c\text{)}$$

$$A_2 = -1.32 + 16.10 \sin 2\left[\frac{2\pi}{360}(\lambda - 45)\right] \quad \text{(A1}d\text{)}$$

$$B_1 = -6.75 + 224.38 \sin\left(\frac{2\pi}{360}\lambda\right) \quad \text{(A1}e\text{)}$$

$$B_2 = -1.04 + 29.76 \cos 2\left[\frac{2\pi}{360}(\lambda - 5)\right] \quad \text{(A1}f\text{)}$$

These values give I_c in units of langleys per day; values of watts per square meter are obtained by multiplying by 0.4846.

The correction for cloud cover is also that suggested by *Reed* [1977]:

$$I = I_c(1. - 0.62C + \alpha) \quad \text{(A2)}$$

where I is the incident solar radiation after the cloud correction (no correction for albedo) and α is the noon solar altitude given by

$$\sin\alpha = \sin\frac{2\pi}{360}(\lambda)\sin\frac{2\pi}{360}\left[23.45° \sin\frac{2\pi}{365}(t - 82)\right] + \cos\frac{2\pi}{360}(\lambda)\cos\frac{2\pi}{360}\left[23.45° \sin\frac{2\pi}{365}(t - 82)\right] \quad \text{(A3)}$$

The final correction is that for albedo, the radiation reflected from the surface. For this we used a constant value

of $A = 0.07$, approximating the mean value found by *Payne* [1972] in spring for the Atlantic Ocean at our latitude:

$$I_0 = (1 - A)I \tag{A4}$$

Although the specific parameterization of solar radiation used here may contain biases in terms of absolute accuracy, radiation is used in the numerical model of vertical mixing, in more of a relative than absolute sense, to determine the interannual differences in solar radiation at the time of the transition.

APPENDIX B: THE NUMERICAL MODEL

The numerical model of vertical mixing used in section 5.5 is that described in detail as the level 2.5 model by *Mellor and Yamada* [1982]. This model solves the equations for conservation of horizontal momentum, salt and heat:

$$\frac{\partial U}{\partial t} = fV + \frac{\partial}{\partial z}\left(K_M \frac{\partial U}{\partial z}\right) \tag{B1a}$$

$$\frac{\partial V}{\partial t} = -fU + \frac{\partial}{\partial z}\left(K_M \frac{\partial V}{\partial z}\right) \tag{B1b}$$

$$\frac{\partial S}{\partial t} = \frac{\partial}{\partial z}\left(K_H \frac{\partial S}{\partial z}\right) \tag{B1c}$$

$$\frac{\partial T}{\partial t} = \frac{\partial}{\partial z}\left(K_H \frac{\partial T}{\partial z}\right) - \frac{1}{\rho c}\frac{\partial I}{\partial z} \tag{B1d}$$

where U and V are the mean eastward and northward velocity, S is the mean salinity, T is the mean temperature, I is the penetrative radiation, ρ and c are water density and specific heat, and f is the Coriolis parameter. These mean quantities are functions of time and depth. Vertical and horizontal advection are neglected in this model, as are horizontal pressure gradients. The assumption implicit in the model is that the vertical turbulent fluxes of momentum, heat, and salt can be expressed as "eddy diffusions," with "eddy diffusivities" given by K_M for momentum and K_H for heat and salt. Other passive scalars can be included in a manner similar to salinity. Density is calculated from temperature and salinity after each time step using an equation of state.

In the above form, the model is a general "K" model. The aspect of the model that identifies it as the Mellor-Yamada level 2.5 model is the manner of specification of K_M and K_H, which are also functions of time and depth. These are given by

$$K_M = lqS_M \qquad K_H = lqS_H \tag{B2}$$

where l is the turbulent length scale and q is the turbulent velocity scale. These are calculated using the differential equations given below. S_M and S_H are functions of the stability of the water column, calculated as algebraic functions of the mean density and velocity fields of the water.

The value of q is calculated at each depth and time by a parameterization of the equation for conservation of turbulent kinetic energy (TKE), expressed as $q^2/2$:

$$\frac{\partial}{\partial t}\frac{q^2}{2} - \frac{\partial}{\partial z}\left[K_q \frac{\partial}{\partial z}\frac{q^2}{2}\right] = P_s + P_b - \varepsilon \tag{B3a}$$

where K_q is a diffusivity for TKE, related algebraically to K_M; P_s, P_b, and ε are shear production of TKE, buoyant production of TKE, and dissipation of TKE, given by

$$P_s = K_M \frac{\partial^2 U}{\partial z^2} + K_M \frac{\partial^2 V}{\partial z^2} \tag{B3b}$$

$$P_b = \frac{g}{\rho} K_H \frac{\partial \rho}{\partial z} \tag{B3c}$$

$$\varepsilon = \frac{q^3}{A_1 l} \tag{B3d}$$

where A_1 is an empirical constant and g is the acceleration of gravity.

To calculate the turbulent length scale l at each depth and time, an equation analogous to that for TKE is formed for the product of TKE and turbulent length scale,

$$\frac{\partial}{\partial t}(q^2 l) - \frac{\partial}{\partial z}\left[K_l \frac{\partial}{\partial z}(q^2 l)\right] = lE_1[P_s + P_b] - \frac{q^3}{B_1}\left\{1 + E_2\left(\frac{l}{kL}\right)^2\right\} \tag{B4}$$

where E_1, E_2, and B_2 are empirical constants and L is a measure of the distance from the nearest surface. See *Mellor and Yamada* [1982] for a complete derivation and discussion of these equations. The boundary conditions at the surface specify that the momentum fluxes are given by the wind stresses, the heat flux is given by the sum of the heat budget terms excluding penetrative radiation, and the salt flux is a function of ambient salinity, precipitation, and evaporation. The turbulent length scale l is assumed to go to zero at the surface; the turbulent velocity scale is found at the surface by setting the parameterizations for shear production and dissipation equal to each other. At the bottom of the domain, all fluxes are assumed to go to zero.

The incident surface visible radiation at the surface is calculated as described in Appendix A. Within the water column, this radiation is described as a double exponential, following *Paulson and Simpson* [1977]:

$$I(z) = [R \exp(z/\zeta_1) + (1 - R) \exp(\zeta_2)]I_0 \tag{B5}$$

where R is the fraction of visible radiation called "longwave," absorbed in a shallow layer with e-folding depth of ζ_1, and the rest is called "shortwave," absorbed with a deeper e-folding depth of ζ_2. Values used here are $R = 0.58$, $\zeta_1 = 0.5$ m and $\zeta_2 = 17.4$ m.

The numerical method of solution for the above equation set is implicit, allowing longer time steps than possible with an explicit method. The time step used here is 30 min. The variables are represented on a vertical grid with approximately 1 m resolution. This grid is compressed into a logarithmic distribution near the surface to increase the resolution near the surface forcing. The vertical domain of the model is 200 m, extending well below the region where the mean quantities are affected by the surface forcing.

Acknowledgments. We thank M. Abbott for access to the CZCS west coast time series, NCAR for the meteorological data, and those responsible for the collection of the CalCOFI data. C. James computed the EOF used as a latitudinal correction in the pigment time series. This work was supported by NASA grant NAGW-1251 and by a Killam Postdoctoral Fellowship (A.C.T.). Modeling was supported by NSF grant OCE-8614026.

REFERENCES

Abbott, M. R., and P. M. Zion, Satellite observations of phytoplankton variability during an upwelling event, *Cont. Shelf Res.*, *4*, 661–680, 1985.

Abbott, M. R., and P. M. Zion, Spatial and temporal variability of phytoplankton pigment off northern California during Coastal Ocean Dynamics Experiment 1, *J. Geophys. Res.*, *92*, 1745–1756, 1987.

Barale, V., and R. W. Fay, Variability of the ocean surface color field in central California near-coastal waters as observed in a seasonal analysis of CZCS imagery, *J. Mar. Res.*, *44*, 291–316, 1986.

Breaker, L. C., and C. N. K. Mooers, Oceanic variability off the central California coast, *Prog. Oceanogr.*, *17*, 61–135, 1986.

Campbell, J. W., and J. E. O'Reilly, Role of satellites in estimating primary productivity on the northwest Atlantic continental shelf, *Cont. Shelf Res.*, *8*, 179–204, 1988.

Chelton, D. B., Large-scale response of the California Current to forcing by wind stress curl, *CalCOFI Rep. 23*, pp. 130–148, Calif. Coop. Oceanic Fish. Invest., Univ. of Calif., San Diego, La Jolla, 1982.

Chelton, D. B., P. A. Bernal, and J. A. McGowan, Large-scale interannual physical and biological interaction in the California Current, *J. Mar. Res.*, *40*, 1095–1125, 1982.

de Szoeke, R. A., and J. G. Richman, On wind-driven mixed layers with strong horizontal gradients—A theory with application to coastal upwelling, *J. Phys. Oceanogr.*, *14*, 363–377, 1984.

Eppley, R. W., E. Stewart, M. R. Abbott, and U. Heyman, Estimating ocean primary production from satellite chlorophyll, Introduction to regional differences and statistics for the Southern California Bight, *J. Plankton Res.*, *7*, 57–70, 1985.

Gordon, H. R., D. K. Clark, J. L. Mueller, and W. A. Hovis, Phytoplankton pigments from the Nimbus-7 coastal zone color scanner: Comparisons with surface measurements, *Science*, *210*, 63–66, 1980.

Gordon, H. R., D. K. Clark, J. W. Brown, O. B. Brown, R. H. Evans, and W. W. Broenkow, Phytoplankton pigment concentrations in the Middle Atlantic Bight: Comparison of ship determinations and CZCS estimates, *Appl. Opt.*, *22*, 20–36, 1983*a*.

Gordon, H. R., J. W. Brown, O. B. Brown, R. H. Evans, and D. K. Clark, Nimbus 7 CZCS: Reduction of its radiometric sensitivity with time, *Appl. Opt.*, *22*, 3929–3931, 1983*b*.

Gordon, H. R., J. W. Brown, and R. H. Evans, Exact Rayleigh scattering calculations for use with the Nimbus-7 coastal zone color scanner, *Appl. Opt.*, *27*, 862–871, 1988.

Haury, L. R., J. J. Simpson, J. Pelaez, C. J. Koblinsky, and D. Wiesenhahn, Biological consequences of a recurrent eddy off Point Conception, California, *J. Geophys. Res.*, *91*, 12,937–12,956, 1986.

Hickey, B. M., The California Current System—Hypotheses and facts, *Prog. Oceanogr.*, *8*, 191–279, 1979.

Huyer, A. E., Coastal upwelling in the California Current System, *Prog. Oceanogr.*, *12*, 259–284, 1983.

Huyer, A. E., and R. L. Smith, The signature of El Niño off Oregon, 1982–1983, *J. Geophys. Res.*, *90*, 7133–7142, 1985.

Huyer, A. E., E. J. Sobey, and R. L. Smith, The spring transition in currents over the Oregon continental shelf, *J. Geophys. Res.*, *84*, 6995–7011, 1979.

Kelly, K. A., Separating clouds from ocean in infrared images, *Remote Sens. Environ.*, *17*, 67–83, 1985.

Kosro, P. M., Structure of the coastal current field off northern California during the Coastal Ocean Dynamics Experiment, *J. Geophys. Res.*, *92*, 1637–1654, 1987.

Landry, M. R., J. R. Postel, W. K. Peterson, and J. Newman, Broad-scale distributional patterns of hydrographic variables on the Washington/Oregon shelf, in *Coastal Oceanography of Washington and Oregon*, edited by M. R. Landry and B. M. Hickey, pp. 1–40, Elsevier, New York, 1989.

Lentz, S., A description of the 1981 and 1982 spring transitions over the northern California shelf, *J. Geophys. Res.*, *92*, 1545–1567, 1987.

Martin, P. J., Simulation of the mixed layer at OWS November and Papa with several models, *J. Geophys. Res.*, *90*, *903–916*, 1985.

McGowan, J. A., El Niño 1983 in the Southern California Bight, in *El Niño North*, edited by W. S. Wooster and D. L. Fluharty, pp. 166–184, Washington Sea Grant Program, University of Washington, Seattle, 1985.

Mellor, G. L., and T. Yamada, Development of a turbulence closure model for geophysical fluid problems, *Rev. Geophys.*, *20*, 851–875, 1982.

Michaelsen, J., X. Zhang, and R. C. Smith, Variability of pigment biomass in the California current system as determined by satellite imagery, 2, Temporal variability, *J. Geophys. Res.*, *93*, 10,883–10,896, 1988.

Mooers, C. N. K., and A. R. Robinson, Turbulent jets and eddies in the California Current and inferred cross-shore transports, *Science*, *223*, 51–53, 1984.

Nelson, C. S., Wind stress and wind stress curl over the California Current, *Rep. NMFS-SSRF-714*, 87 pp., Natl. Oceanic and Atmos. Admin., Monterey, Calif., 1977.

Nelson, C. S., and D. M. Husby, Climatology of surface heat fluxes over the California Current region, *Rep. NMFS-SSRF-763*, 155 pp., Natl. Oceanic and Atmos. Admin., Monterey, Calif., 1983.

Niiler, P. P., and E. B. Kraus, One-dimensional models of the upper ocean, in *Modelling and Prediction of the Upper Layers of the Ocean*, edited by E. B. Kraus, pp. 143–172, Pergamon, New York, 1977.

Parsons, T. R., L. F. Giovando, and R. J. LeBrasseur, The advent of the spring bloom in the eastern subarctic Pacific Ocean, *J. Fish. Res. Board Can.*, *23*, 539–546, 1966.

Paulson, C. A., and J. J. Simpson, Irradiance measurements in the upper ocean, *J. Phys. Oceanogr.*, *7*, 952–956, 1977.

Payne, R. E., Albedo of the sea surface, *J. Atmos. Sci.*, *29*, 959–970, 1972.

Pelaez, J., and J. A. McGowan, Phytoplankton pigment patterns in the California Current as determined by satellite, *Limnol. Oceanogr.*, *31*, 927–950, 1986.

Price, J. F., R. A. Weller, and R. Pinkel, Diurnal cycling: Observations and models of the upper ocean response to diurnal heating, cooling, and wind mixing, *J. Geophys. Res.*, *91*, 8411–8427, 1986.

Reed, R. K., On estimating insolation over the ocean, *J. Phys. Oceanogr.*, *7*, 482–485, 1977.

Rienecker, M. M., C. N. K. Mooers, D. E. Hagan, and A. R. Robinson, A cool anomaly off northern California: An investigation using IR imagery and in situ data, *J. Geophys. Res.*, *90*, 4807–4818, 1985.

Riley, G. A., Phytoplankton in the north central Sargasso Sea 1950–52, *Limnol. Oceanogr.*, *2*, 252–270, 1957.

Scripps Institution of Oceanography (SIO), Physical, chemical and biological data report, *SIO Ref. 84-23*, Univ. of Calif., La Jolla, 1984.

Scripps Institution of Oceanography (SIO), Physical, chemical and biological data report, *SIO Ref. 85-14*, Univ. of Calif., La Jolla, 1985.

Seckel, G. R., and F. H. Beaudry, The radiation from sun and sky over the North Pacific Ocean (abstract), *Eos Trans. AGU. 54*, 1114, 1973.

Small, L. F., and D. W. Menzies, Patterns of primary productivity and biomass in a coastal upwelling region, *Deep Sea Res.*, *28*, 123–149, 1981.

Smith, R. C., X. Zhang, and J. Michaelsen, Variability of pigment biomass in the California Current System as determined by satellite imagery, 1, Spatial variability, *J. Geophys. Res.*, *93*, 10,863–10,882, 1988.

Strub, P. T., and C. James, Atmospheric conditions during the spring and fall transitions in the coastal ocean off western United States, *J. Geophys. Res.*, *93*, 15,561–15,584, 1988.

Strub, P. T., J. S. Allen, A. Huyer, and R. L. Smith, Large-scale structure of the spring transition in the coastal ocean off western North America, *J. Geophys. Res.*, *92*, 1527–1544, 1987*a*.

Strub, P. T., J. S. Allen, A. Huyer, R. L. Smith, and R. C. Beardsley, Seasonal cycles of currents, temperatures, winds, and sea level over the northeast Pacific continental shelf: 35°N to 48°N, *J. Geophys. Res.*, *92*, 1507–1526, 1987*b*.

Sverdrup, H. U., On conditions for the vernal blooming of phytoplankton, *J. Cons. Int. Explor. Mer*, *18*, 287–295, 1953.

Thomas, A. C., and W. J. Emery, Winter hydrography and plankton distributions on the southern British Columbia shelf, *Can. J. Fish. Aquat. Sci.*, *43*, 1249–1258, 1986.

Thomas, A. C., and W. J. Emery, Relationships between near-surface plankton concentrations, hydrography, and satellite-measured sea surface temperature, *J. Geophys. Res.*, *93*, 15,733–15,748, 1988.

Woodruff, S. D., R. J. Slutz, R. L. Jenne, and P. M. Steurer, A comprehensive ocean-atmosphere data set, *Bull. Am. Meteorol. Soc.*, *68*, 1239–1250, 1987.

P. T. Strub and A. C. Thomas, College of Oceanography, Oregon State University, Corvallis, OR 97331.

(Received March 3, 1989;
revised June 13, 1989;
accepted June 16, 1989.)